

Neurodynamical Role of STDP in Storage and Retrieval of Associative Information

Hongkyu Yoon* and Pilwon Kim†

Department of Mathematical Sciences
Ulsan National Institute of Science and Technology(UNIST)
Ulsan Metropolitan City
44919, Republic of Korea

January 22, 2022

Abstract

Spike-timing-dependent plasticity (STDP) is a biological process in which the precise order and timing of neuronal spikes affect the degree of synaptic modification. While there has been numerous research focusing on the role of STDP in neural coding, the functional implications of STDP at the macroscopic level in the brain have not been fully explored yet. In this work, we propose that STDP in an ensemble of spiking neurons renders storing high dimensional information in the form of a ‘memory plane’. Neural activity based on STDP transforms periodic spatio-temporal input patterns into the corresponding memory plane, where the stored information can be dynamically revived with a proper cue. Using the dynamical systems theory that shows the analytic relation between the input and the memory plane, we were able to demonstrate a specific memory process for high-dimensional associative data sets. In the auto-associative memory task, a group of images that were continuously streamed to the system can be retrieved from the oscillating neural state. The second application deals with the process of semantic memory components that are embedded from sentences. The results show that words can recall multiple sentences simultaneously or one exclusively, depending on their grammatical relations. This implies that the proposed framework is apt to process multiple groups of associative memories with a composite structure.

Spike-timing-dependent plasticity (STDP), as a synaptic modification rule according to the order of pre- and post-synaptic spiking within a critical time window, has been demonstrated in the nervous systems over a wide range of species from insects to humans. STDP is considered to be critical for understanding the cognitive mechanisms such as learning of temporal sequences [1, 2], formation of associative memory [3, 4] and manipulation of existing memory [5, 6, 7]. Despite such progress and findings, the question still remains open as to how STDP affects the distributed process of information at the macroscopic level in the brain.

Modeling macroscopic brain activity with nonlinear dynamical systems facilitates understanding of brain functions [8, 9, 10]. The hypothesis of storing memory in a form of an attractor of the

*hkyoon@unist.ac.kr

†pwkim@unist.ac.kr, *correspondence*

dynamics is now accepted with substantial supporting evidence [11, 12, 13, 14, 15, 16]. However, it is still unclear how specific trajectories of neural states could emerge through neural plasticity. While the Hopfield network and other variants have attempted to encode memory to a fixed point attractor, they have little in common with actual brain dynamics which is based on oscillatory synchronization.

When excited by a repeating sequence, STDP can create a circular set of directed connections inducing neural oscillations. The limit cycles in the neural state space have been considered to be involved in many functions including long- and short-term memory and storage of multiple memory components [17, 18, 19, 20, 21].

In this work, we analyze an STDP-based neural model and show that the model can associate multiple high-dimensional memories to a geometric structure in the neural state space which we call a memory plane. When exposed to repeatedly occurring spatio-temporal input patterns, neural activity based on STDP transforms the patterns into the corresponding memory plane. In the retrieval phase, the memory plane plays a role of a generator of a limit cycle in reaction to a recall cue. The stored memories can be dynamically revived around the memory plane if perturbed by a similar stimulus.

The presence and the function of the memory plane in the neural networks have caught attention in [22], where it has been proposed that STDP can store transient inputs as imaginary-coded memories. In this work, we further emphasize an active role of the memory plane in both theory and practice, showing that it can play a central role in storing, retrieving, and manipulating practical information. We intend to integrate an analytic and an implementation level description of the neuronal memory process based on the memory plane that is capable of handling high dimensional associative data. Using the dynamical systems theory, we derive an analytic relation between the input, the memory plane, and the induced limit cycles. In the numerical task, a group of images is continuously carried by an oscillating impulse and streamed into the system for storage. The set of whole images can be dynamically retrieved as predicted when perturbed by a proper recall cue. The quality of retrieved images depends on how much the cue reflects one of the original images.

Furthermore, the proposed memory system provides a plausible algorithmic basis by which separate groups of associated memory components can be learned. We use multiple semantic vectors as the memory input to the system, each of which represents a sentence as a composite of words. The results show that a word can recall multiple sentences simultaneously or one exclusively, depending on their grammatical relations. This implies that the proposed framework is apt to process multiple groups of associative memories with composite structure.

Results

Model

Following the standard firing-rate models [23, 22], we set the differential equation for the neural state as

$$\dot{\mathbf{x}} = -\mathbf{x} + \mathbf{W}\phi(\mathbf{x}) + \mathbf{b}(t), \quad (1)$$

where $\mathbf{x} = [x_1 \ x_2 \ \dots \ x_N]^\top \in \mathbb{R}^N$ is the state of N neuronal nodes and $\mathbf{W} = (W_{ij}) \in \mathbb{R}^{N \times N}$ is a connectivity matrix with W_{ij} corresponding to the strength of synaptic connection from node j to i . Here ϕ is a regularizing transfer function and $\mathbf{b}(t)$ is a memory input.

The mechanism of STDP can be formulated as [24]

$$\begin{aligned} \dot{W}_{ij}(t) = -\gamma W_{ij}(t) + \rho \left(\underbrace{\int_0^\infty K(s)\phi(x_j(t-s))\phi(x_i(t)) \, ds}_{\text{pre-synaptic STDP}} \right. \\ \left. + \underbrace{\int_{-\infty}^0 K(s)\phi(x_i(t+s))\phi(x_j(t)) \, ds}_{\text{post-synaptic STDP}} \right), \end{aligned} \quad (2)$$

where K is a temporal kernel. Here γ and ρ are the decaying rate of homeostatic plasticity and the learning rate, respectively, and we assume that they are positive during memory storage and become negligible during memory retrieval.

For analytic simplicity, we use $\phi(\mathbf{x}) = \mathbf{x}$ and a Dirac-delta kernel $K(s)$ defined as

$$K(s) := \begin{cases} \delta(s - s_0) & s > 0 \\ -\delta(s + s_0) & s \leq 0, \end{cases} \quad (3)$$

with $s_0 > 0$. After simplifications, the main model becomes

$$\begin{cases} \dot{\mathbf{x}} = -\mathbf{x} + \mathbf{W}\mathbf{x} + \mathbf{b}(t) \\ \dot{\mathbf{W}} = -\gamma\mathbf{W} + \rho(\mathbf{x}\mathbf{x}_\tau^\top - \mathbf{x}_\tau\mathbf{x}^\top), \end{cases} \quad (4)$$

where $\mathbf{x}_\tau = \mathbf{x}(t - \tau)$ stands for delayed synaptic response. More detailed derivation of the evolution rule for \mathbf{W} in Eq. (4) can be found in the supplementary material.

Encoding with tag vectors

It is reasonable to assume that the cognitive systems do not simply receive an external input in a passive way, but rather actively pose it in the neural state space on acceptance. Let $\mathbf{f}_1, \dots, \mathbf{f}_n \in \mathbb{R}^M$ be a series of the external inputs from the environment containing high dimensional associative information. We use a set of internal tags $\mathbf{r}_1, \dots, \mathbf{r}_m$ to mark what classes the corresponding external input belongs to. They may be used to indicate the order of sequence for the events (the first, the second, \dots , the last) if the input is streamed through sequential observations, or types of sensors (visual, auditory, olfactory, tactile) if the input is a combination of senses, or the sentence elements (subject, predicate, object, modifier) if the input is a sentence composed of words. Such internal tags $\mathbf{r}_1, \dots, \mathbf{r}_m$ can be formulated as low dimensional orthonormal vectors.

Now we use the tensor product to encode an external input \mathbf{f}_i into a *memory component* \mathbf{m}_i as

$$\mathbf{m}_i = \mathbf{f}_i \otimes \mathbf{r}, \quad (5)$$

where \mathbf{r} is the tag vector that corresponds to the external input \mathbf{f}_i . If \mathbf{r} is of unit length, the original external input can be exactly decoded from the memory components by applying the tagging vector by

$$\mathbf{m}_i \cdot \mathbf{r} = (\mathbf{f}_i \otimes \mathbf{r}) \cdot \mathbf{r} = \mathbf{f}_i(\mathbf{r} \cdot \mathbf{r}) = \mathbf{f}_i. \quad (6)$$

Storage phase

We assume that multiple memory components $\mathbf{m}_1, \dots, \mathbf{m}_n$ are fed into the system (4) through the harmonic pulse as

$$\mathbf{b}(t) = \sum_{i=1}^n \sin(\omega t - \xi_i) \mathbf{m}_i. \quad (7)$$

Here ω stands for the frequency of neural oscillations and ξ_i , $i = 1, \dots, n$ stands for the sampling time for each component.

It can be shown that the trajectory of the memory input $\mathbf{b}(t)$ in (7) is periodic and embedded in a 2-dimensional plane in \mathbb{R}^N , which is located in a subspace spanned by each memory components $\mathbf{m}_1, \dots, \mathbf{m}_n$. We define such plane as a *memory plane* S with respect to the memory components. While the memory components are distributed in the extremely high dimensional neural state space \mathbb{R}^N , the memory plane S is located in close proximity to the memory components. Especially if the memory components are of the same magnitude and the sampling time ξ_i is evenly sequenced on interval $[0, \pi]$, one can show the angle between the memory component \mathbf{m}_i and S is bounded as

$$|\theta_i| \leq \cos^{-1} \left(\sqrt{\frac{2}{n}} \right), \quad i = 1, \dots, n. \quad (8)$$

The equality holds when the memory components are mutually orthogonal.

The following theorem shows that STDP mechanism in Eq. (4) captures the dynamics of $\mathbf{b}(t)$ and stores the information about the corresponding memory plane S into the connectivity matrix \mathbf{W} .

Theorem 1. *The system (4) under the memory input (7) has a periodic solution $\mathbf{x}(t)$ on the memory plane S with a constant connectivity matrix $\mathbf{W}(t) = \mathbf{W}^* \in \wedge^2(S)$.*

Here $\wedge^2(S)$ indicates an exterior power of S , which is a set of matrices in the form of $\mathbf{v}\mathbf{u}^\top - \mathbf{u}\mathbf{v}^\top$ for any vectors \mathbf{u} and \mathbf{v} in S . Further analysis on the Lyapunov exponent shows that there exists a decent ranges of the parameters where the corresponding solution $\mathbf{x}(t)$ in Theorem 1 is asymptotically stable. More detailed forms of S , \mathbf{W}^* and $\mathbf{x}(t)$ can be found in the proof of the theorem in the supplementary material. In the following sections, we will show that the memory plane S successfully characterizes the associative memory composed of $\mathbf{m}_1, \dots, \mathbf{m}_n$, and further that oscillations of the neural state $\mathbf{x}(t)$ around S can be used for dynamic memory retrieval.

Retrieval phase

In the retrieval phase, we assume that $\gamma = \rho = 0$ in Eq. (4) and the connectivity matrix \mathbf{W} is frozen at \mathbf{W}^* which is attained during the storage phase as in Theorem 1. Then the retrieval phase is governed by the equation

$$\dot{\mathbf{x}} = -\mathbf{x} + \mathbf{W}^* \mathbf{x} + \mathbf{b}(t). \quad (9)$$

We are interested in how much information on the memory components $\mathbf{m}_1, \dots, \mathbf{m}_n$ can be retrieved from the dynamics of $\mathbf{x}(t)$, while $\mathbf{x}(t)$ is externally excited by the memory input

$$\mathbf{b}(t) = \sin \omega t \mathbf{m}_c, \quad (10)$$

where \mathbf{m}_c is the memory cue. Once the solution $\mathbf{x}(t)$ approaches a certain oscillation, then retrieval of the information can be performed by applying the tag vectors to $\mathbf{x}(t)$, as $\mathbf{x}(t) \cdot \mathbf{r}_j$, $j = 1, \dots, m$. This produces continuously evolving retrieval along the oscillation.

The following theorem suggests that if \mathbf{m}_c is given close to one of the memory components, the resulted neural oscillation occurs near the memory plane, and therefore in close proximity to all the memory components.

Theorem 2. *Suppose the memory cue \mathbf{m}_c is not orthogonal to the memory plane S . Then $\mathbf{x}(t)$ in Eq. (9) with Eq. (10) converges to a periodic solution that passes through S .*

Note that the neural state space is so high dimensional that a random choice for \mathbf{m}_c is likely to be orthogonal to S . Fig. 1 provides an insight into the role of the memory plane S in the retrieval dynamics. The memory components $\mathbf{m}_1, \dots, \mathbf{m}_m$ are pictured as gathered in a relatively small region to make a visual contrast to the vastness of the neural state space \mathbb{R}^N . The memory plane S is located in the subspace spanned by the memory components. When the given memory cue \mathbf{m}_c is relevant to the stored memory components, the memory plane S plays a role of a generator of a limit cycle for the neural state $\mathbf{x}(t)$ to circle around the memory components.

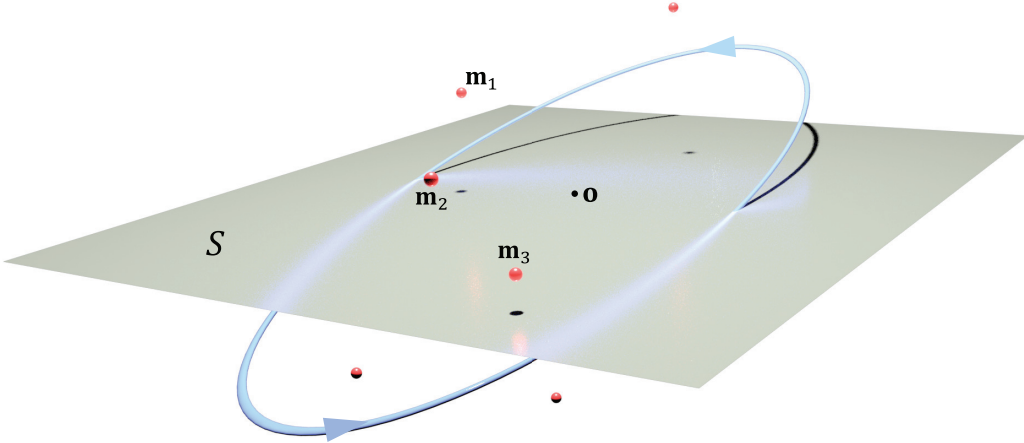


Figure 1: Graphical illustration of the memory components $\mathbf{m}_1, \dots, \mathbf{m}_n$ and the corresponding memory plane S . The memory plane S is located in the subspace spanned by the memory components and is shown to be close enough to them. A periodic orbit close to S can be used for efficient memory retrieval.

Numerical Simulations

Retrieval of grouped images

We first demonstrate an auto-associative memory task that involves a group of images. This task uses five 64×64 grayscale images of classical orchestral instruments in Fig. 2. The images are translated into external input vectors \mathbf{f}_i , $i = 1, \dots, 5$ in \mathbb{R}^{64^2} and are combined into the memory components as $\mathbf{m}_i = \mathbf{f}_i \otimes \mathbf{r}_i$, $i = 1, \dots, 5$. Here the tag vectors \mathbf{r}_i , $i = 1, \dots, 5$ are orthonormal in \mathbb{R}^5 and used as a placeholder for each image.

Fig. 3 depicts the numerical simulation for the retrieval phase. For a better understanding of the process, a graphic illustration of the memory plane and the initial memory cue is given with the actual data. When the neural state $\mathbf{x}(t)$ in Eq. (5) is continually perturbed by a noisy copy of one of the original images (violin), it approaches the memory plane S . Once the $\mathbf{x}(t)$ converges

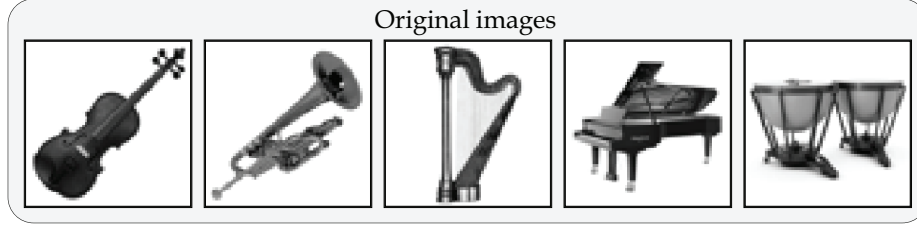


Figure 2: Grayscale images of 64×64 pixels displaying classical orchestral instruments that are used for the memory input vectors $\mathbf{f}_1, \dots, \mathbf{f}_5$.

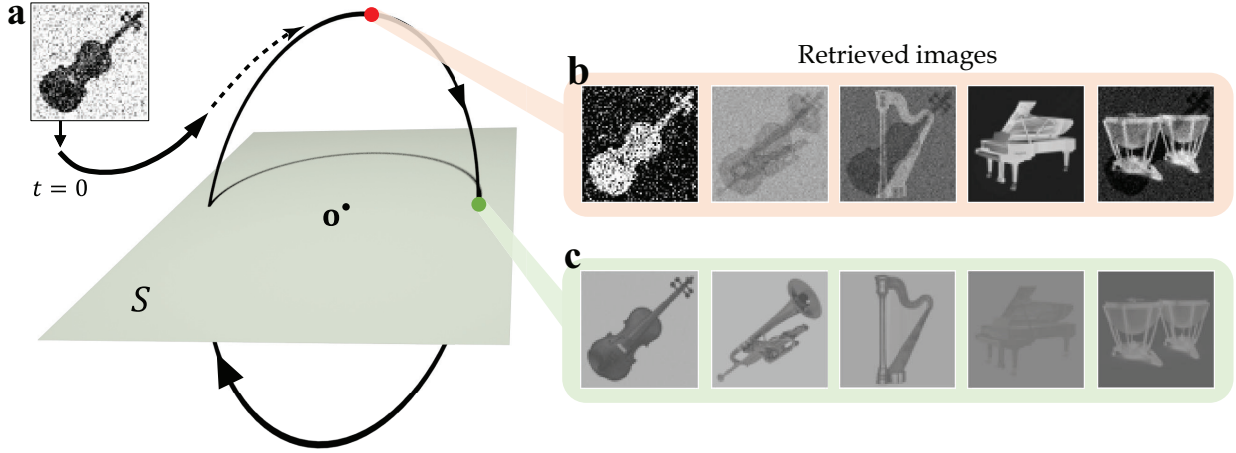


Figure 3: Auto-associative memory retrieval from a contaminated cue. **(a)** The noisy cue $\mathbf{m}_c = \tilde{\mathbf{f}}_1 \otimes \tilde{\mathbf{r}}_1$ is generated from $\tilde{\mathbf{f}}_1 = \sqrt{1 - \alpha^2} \mathbf{f}_1 + \alpha \boldsymbol{\zeta}$ and $\tilde{\mathbf{r}}_1 = \sqrt{1 - \beta^2} \mathbf{r}_1 + \beta \boldsymbol{\eta}$, where $\boldsymbol{\zeta}, \boldsymbol{\eta}$ are Gaussian noise following $\mathcal{N}_{\mathbb{R}^{64^2}}(0, \|\mathbf{f}_1\|)$ and $\mathcal{N}_{\mathbb{R}^5}(0, 1)$, respectively. The parameters are $\alpha = 0.25$ and $\beta = 0.2$. **(b)** Snapshot of the retrieved images at the farthest point (red dot) from memory plane S . **(c)** Snapshot of the retrieved images at the intersection (green dot) of the orbit and the memory plane S .

to a limit cycle around S as stated in Theorem 2, the external input $\mathbf{f}_1, \dots, \mathbf{f}_5$ can be reproduced by applying the tag vectors to $\mathbf{x}(t)$. In Fig. 3, we display two snapshots of the retrieved images obtained at two points on the orbit: Fig. 3b is taken at the farthest from S and Fig. 3c is at the intersection. It is notable that the retrieved images continuously oscillate, developing weak/strong and positive/negative images in turns. Such flashing patterns are generally different from image to image and are affected by the sequential order of the memory components in Eq. (7) in the storage phase. Furthermore, due to the orthogonality of the tag vectors, the perfect images are acquired on the time instance when $\mathbf{x}(t)$ penetrates S .

Fig. 4 shows that the quality of the retrieved images depends on how close the memory cue is to the original image input. The cue with low-level noise in Fig. 4a leads to the orbit (blue) close to the memory plane S , producing the images of decent quality in Fig. 4c. However, if the cue is more contaminated with noise as in Fig. 4b, $\mathbf{x}(t)$ approaches S at a relatively larger angle, making a stretched narrower elliptical orbit (red) that periodically gets far from S . Although the orbit from the severely contaminated cue still passes through the memory plane, it only does near the origin, providing relatively feeble images during a short time.

The retrieval can be performed with an incomplete cue. In Fig. 5a, the images are recalled from

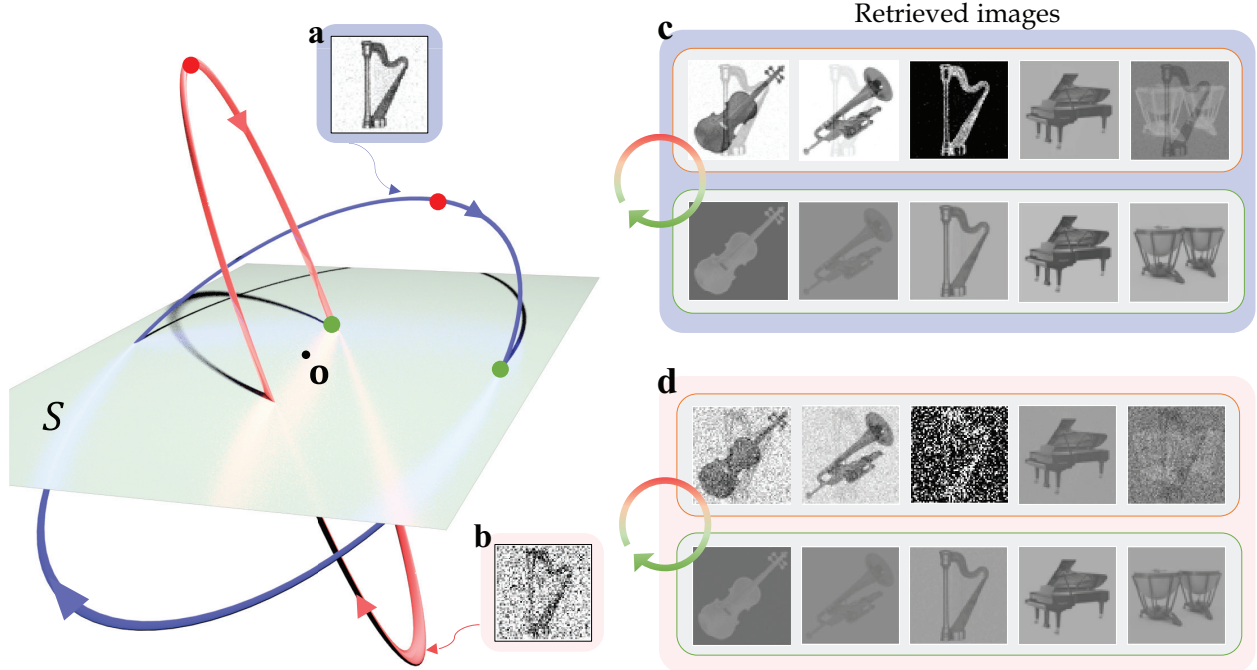


Figure 4: Comparison of retrieval quality according to the noise level in the cue. **(a)** The less noisy cue. The cue is generated in the same way as in Fig. 3 except using f_3 and r_3 instead of f_1 and r_1 . Gaussian noise are $\mathcal{N}_{\mathbb{R}^{642}}(0, \|f_3\|)$ and $\mathcal{N}_{\mathbb{R}^5}(0, 1)$, respectively. The parameters are $\alpha = 0.1$ and $\beta = 0.2$. **(b)** The severely contaminated cue with $\alpha = 0.7$. **(c)** Snapshots of the retrieved images from the less noisy cue in (a), taken at the farthest point from S (top row) and at the intersection (bottom row). **(d)** Snapshots of the retrieved images from the more noisy cue in (b), taken at the farthest point from S (top row) and at the intersection (bottom row).

the partially obstructed cue. The original images can be recovered at a decent level, especially when $x(t)$ passes through the memory plane S . Fig. 5b displays that an irrelevant cue (forest) fails to retrieve the original memory inputs. Indeed, it can be shown that a completely irrelevant cue results in a one-dimensional periodic orbit that keeps penetrating the memory plane back and forth just at the origin.

Multiple groups of memory with composite structure

This section deals with applications of the model to more complex associative memory. Suppose we have multiple groups of memory components and have stored each group in the form of the memory plane using the system in Eq. (4). We are especially interested in the case where some memory components belong to multiple groups. The following questions naturally arise: 1) Can the common memory component retrieve the corresponding multiple groups together? 2) Can a single memory group be selected by adding a further memory component in the cue? These questions are potentially related to high-level inference on memory.

We also focus on compositional structure of memory components created by the tag vectors. Memory inputs in this section are words and are collectively provided in the form of a sentence. We assume that each tag vector stands for the sentence element (subject, predicate, object, modifier) and is naturally bound to a word according to the role of the corresponding word in the sentence. Being activated by such a sequential stream of words, the system in Eq. (4) forms the memory

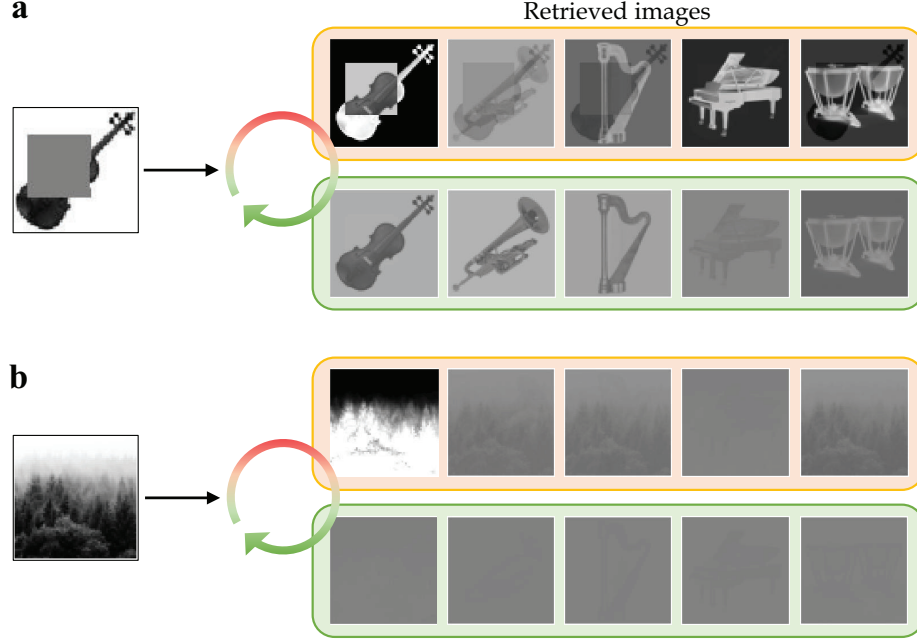


Figure 5: **(a)** Result of retrieval from a partially obstructed cue. Snapshots of the retrieved images are taken at the farthest point from S (top row) and at the intersection of the orbit and the memory plane (bottom row). **(b)** Result of retrieval from an irrelevant cue. Snapshots of the retrieved images are taken at the farthest point from S (top row) and at the intersection of the orbit and the memory plane (bottom row). In both (a) and (b), we used the noisy tag vector $\tilde{\mathbf{r}}_1$ used in Fig. 3 for retrieval.

plane which can be referred to as the encoding of the sentence.

For the simulation of semantic memory, we use three sentences composed of 8 words. Every word appearing in the sentence has one of the 4 roles (sentence elements). The vocabulary of the words and the roles are listed in Fig. 6a. We simply use arbitrarily chosen orthonormal sets $\{\mathbf{f}_i\}_{i=1}^8$ for the words and $\{\mathbf{r}_j\}_{j=1}^4$ for the roles, respectively. Fig. 6b shows a couple of examples for memory components each of which is a binding of a word and a role. Here the subindex on the right-hand side is used to express the corresponding role for the word. Our goal is to store the semantic information of sentences through Eq. (4) with the memory input $\mathbf{b}(t)$ in Eq. (7). There are three sentences S_1, S_2 and S_3 listed in Fig. 6c that we use as the memory input in the simulation. Note that word **John** appears three times in the sentences, once in S_1 as an object, and twice in S_2 and S_3 as a subject. Similarly, the words **Mary** and **garden** occur twice in a different context.

The memory connectivity \mathbf{W}_k^* , $k = 1, 2, 3$ are obtained from separate single group learning on the sentences S_k , $k = 1, 2, 3$, respectively. We then set the combined memory connectivity for three sentences, i.e., $\mathbf{W}^* = \mathbf{W}_1^* + \mathbf{W}_2^* + \mathbf{W}_3^*$ for the collective retrieval phase. We adopt the function

$$P_j^i(t) := \int_{t_0}^t |\mathbf{f}_i^\top(\mathbf{x}(t) \cdot \mathbf{r}_j)| ds, \quad i = 1, \dots, 8, \quad j = 1, \dots, 4, \quad (11)$$

to measure how close the retrieved quantity is to the word \mathbf{f}_i as the role \mathbf{r}_j .

In the first task of multiple composite memories, **Mary**_S is given as the cue. Since **Mary** occurs as a subject only in S_1 , one can expect the retrieved result to be S_1 as in Fig. 7a. The numerical simulation of the retrieval process turned out to agree well with this expectation. Fig. 7b compares the fitness of the words. The values of $P_j^i(t)$ in Eq. (11) are evaluated while $\mathbf{x}(t)$ is oscillating

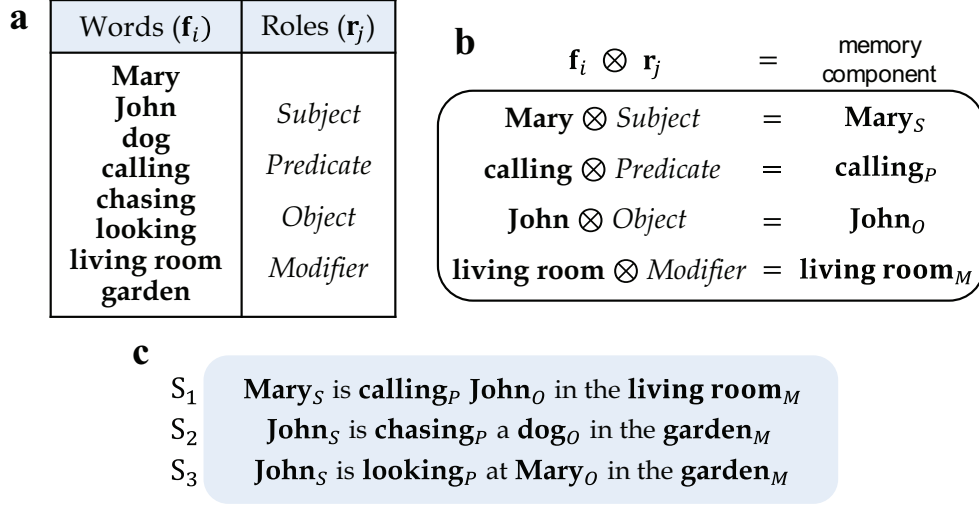


Figure 6: (a) List of words and roles used for the external input \mathbf{f}_i and the tag \mathbf{r}_j . (b) Descriptive explanation on constructing memory components. (c) Three sentences S₁, S₂ and S₃ generated by grouping memory components. Note that the words **John**, **Mary** and **garden** appear several times in different contexts.

along a convergent orbit of Eq. (9). If $P_j^i(t)$ keeps increasing with a large slope, the corresponding memory component $\mathbf{f}_i \otimes \mathbf{r}_j$ can be identified as a dominantly retrieved one. The graphs in Fig. 7b show that such components are **Mary_S**, **calling_P**, **John_O** and **living room_M**, which are well matched to S₁.

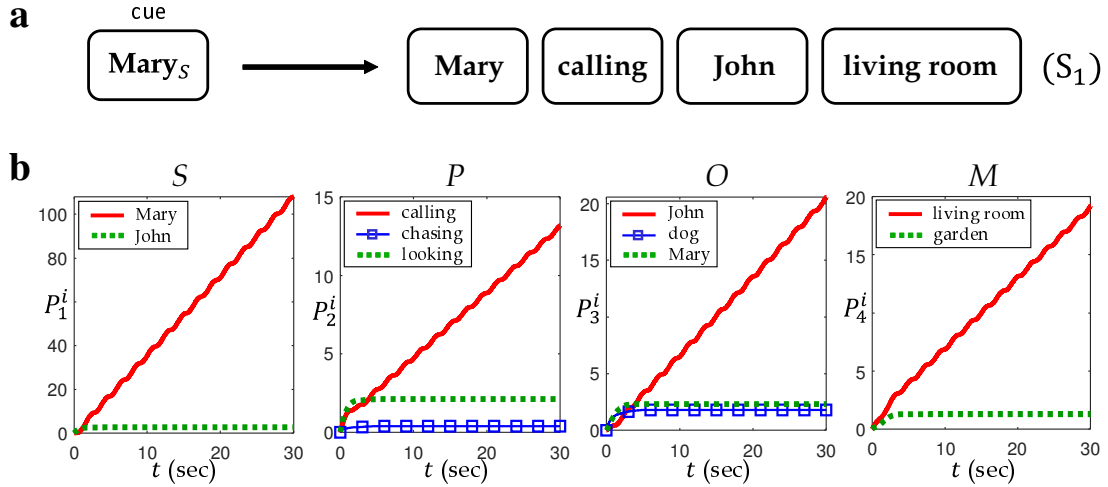


Figure 7: (a) Expected result of retrieval when the cue **Mary_S** is given. (b) The numerical result of retrieval by the cue **Mary_S**. Dominant increasing values of $P_i^j(t)$ are colored red, which turned out to correspond to S₁.

The second task deals with the case with an ambiguous memory cue. Suppose that the memory component **John_S** is given as the cue. Since it occurs in the both sentence S₂ and S₃, it is reasonable that the retrieval result should involve all the memory components in both sentences as in Fig. 8a. This may be understood in that one of the fundamental capabilities of the brain is to examine

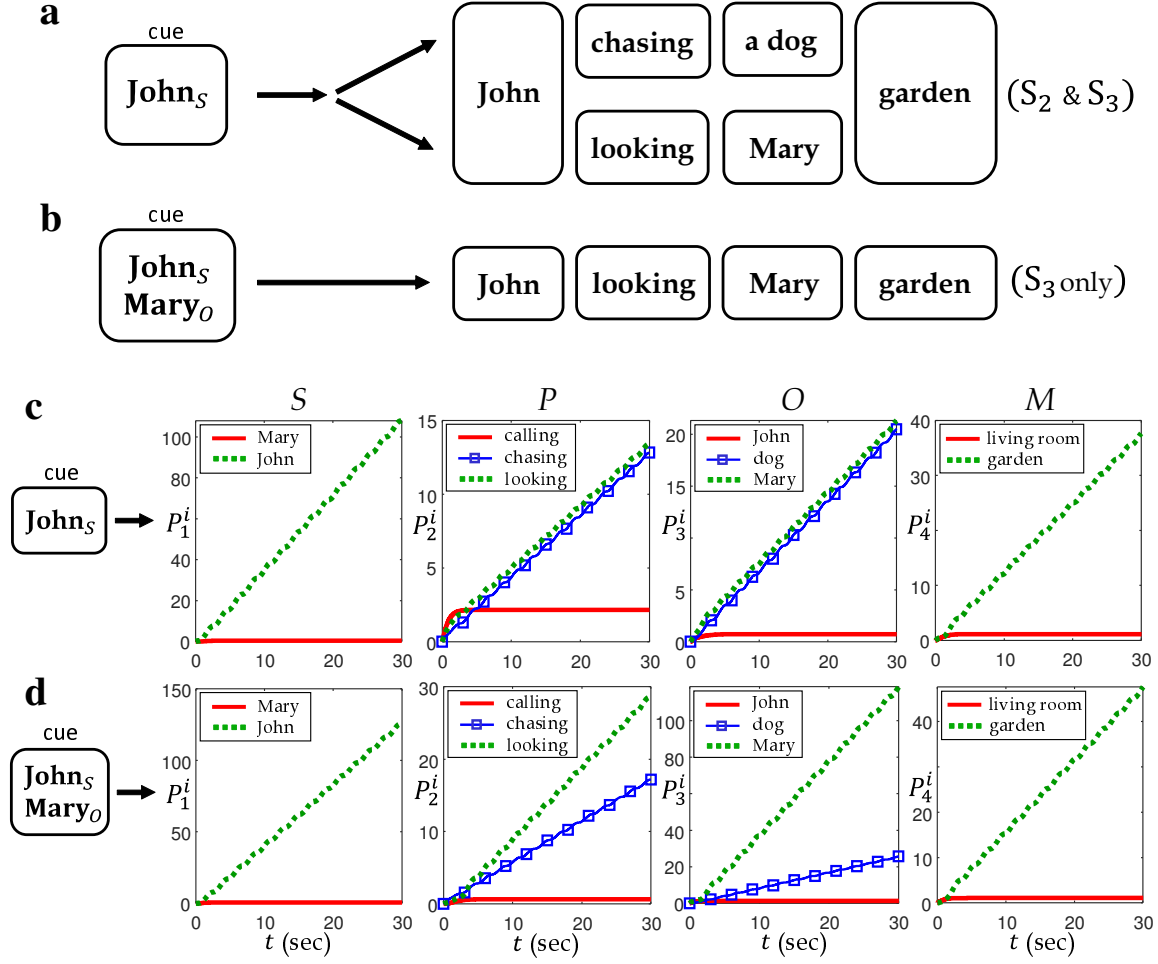


Figure 8: **(a)** Expected result of retrieval by a single component cue John_S . **(b)** Expected result of retrieval by multiple component cues John_S and Mary_O . **(c)** Numerical result of retrieval by a single component cue John_S . **(d)** Numerical result of retrieval by multiple component cues John_S and Mary_O .

all possible memories that contain the common cue, especially when the given cue is insufficient. However, this ambiguity can be eliminated by adding further cues. For example, if Mary_O is added as in Fig. 8b, the retrieval result should be narrowed down to S_3 due to the extra constraint.

It turned out that the numerical simulations successfully capture the expected features of the memory retrieval process mentioned above. Fig. 8c shows the results from the memory cue John_S . It is notable that chasing_P and looking_P in the second graph simultaneously increase with the almost same slope, indicating that they are equally dominant memory components in retrieval. This is even clearer when compared to another memory component calling_P which is steady and negligible. The same pattern appears with John_O and dog_O in the third graph, both of which are dominant retrieval components. The numerical results in Fig. 8d also reflect the retrieval tendency with additional memory cue. We provide the system in Eq. (9) with the extended memory input in Eq. (10) that consists of two memory components John_S and Mary_O . Since the newly added cue Mary_O confines the retrieval result to the sentence S_3 as in Fig. 8b, the memory components in S_2 , chasing_P and dog_O , should be suppressed in retrieval. The second and third graphs in Fig. 8d show that, while chasing_P and dog_O increase (due to the common cue John_S), the slope is

smaller than that of **looking**_P and **Mary**_O in S_3 , respectively. This implies that the dominantly retrieved components are **John**_S, **looking**_P, **Mary**_O and **garden**_M which are matched to S_3 .

Discussion

There is now substantial evidence accumulated that neural oscillations are related to memory encoding, attention, and integration of visual patterns [25, 26, 27]. In [22], the idea has been proposed that memories constitute stable dynamical trajectories on a two-dimensional plane in which an incoming stimulus is encoded as a pair of imaginary eigenvalues in the connectivity matrix. We extend such an idea further through a specific memory system that can process a group of high dimensional associative data sets, by proving the exact relation between the inputs and the corresponding synaptic changes. In the proposed model, macroscopic neural oscillations in the brain can be viewed as natural activities occurring during the storage and retrieval of information. Using the dynamical systems theory, we rigorously derived a specific form of the two-dimensional memory plane in terms of the given data sets. Different from the Hopfield network that retrieves static single data as a fixed point, the proposed model produces neural oscillations in response to an external cue, exploring various aspects of stored multiple data sets around the memory plane.

We encode the input data with tag vectors based on the tensor representation. This preprocess enables us to efficiently retrieve the stored data and, in addition, to deal with the composite structure in the data set. While its biological realization in cognitive architecture is still a controversial issue, the tensor-based composition has been proposed as a robust and flexible distributed memory representation [28, 29, 30, 31, 32]. The ability to process associate multiple data sets with composite structures is essential in natural-language understanding and reasoning. It has been shown that the proposed model can handle multiple sentences that describe distinct situations and can selectively allow the recall cue to arouse a group of associative memories according to its semantic relevance.

From a practical perspective, our results suggest an alternative approach for a memory device. The conventional von Neumann architecture is non-scalable and its performance is limited by the so-called von Neumann bottleneck between nonvolatile memories and microprocessors. On the other hand, operating data with artificial synapses is benefiting from a parallel information process consuming a small amount of energy per synapse. Moreover, conventional digital memory systems convert the inputs to a binary code and save it in a separate storage device, likely destroying the correlation information by such physical isolation. The proposed model is based on continuous dynamical systems and provides a simple and robust approach to deal with a sequence of associative high-dimensional data. Processing data in the continuous and distributed system results in the plastic storage of the correlated information in the synaptic connections.

Methods

Encoding and Decoding of Memory Components

For an input vector $\mathbf{f} \in \mathbb{R}^D$ and a tag $\mathbf{r} = [r_1, \dots, r_K]^T \in \mathbb{R}^K$, the corresponding memory component $\mathbf{m} = [m_1, \dots, m_{DK}]^T \in \mathbb{R}^{DK}$ is defined as the flattened vector form of $\mathbf{f} \otimes \mathbf{r}$ in which the vectors $r_1\mathbf{f}, \dots, r_K\mathbf{f}$ are vertically aligned. Then the right dot product in the retrieval process is computed as $\mathbf{m} \cdot \mathbf{r} = \mathbf{M}\mathbf{r}$, where $\mathbf{M} \in \mathbb{R}^{D \times K}$, $(\mathbf{M})_{ij} = m_{i+D(j-1)}$, $1 \leq i \leq D$, $1 \leq j \leq K$.

The benefit of using orthonormal tag vectors \mathbf{r}_i is that they achieve clear selective recovery of the original \mathbf{f}_i when the neural state \mathbf{x} is expressed as a linear combination of the memory components:

$$\left(\sum_{j=1}^n c_j \mathbf{m}_j \right) \cdot \mathbf{r}_i = \left(\sum_{j=1}^n c_j (\mathbf{f}_j \otimes \mathbf{r}_j) \right) \cdot \mathbf{r}_i = \sum_{j=1}^n c_j \mathbf{f}_j (\mathbf{r}_j \cdot \mathbf{r}_i) = c_i \mathbf{f}_i. \quad (12)$$

Model Simulation*

For numerical simulations in this article, the modified Euler’s method for delay equations has been universally used. In the first memory task, each 64×64 image is translated to a vector \mathbf{f}_i as follows: every pixel is mapped to a value in $[-\sigma, \sigma]$, $\sigma > 0$, depending on its brightness (pure black to $-\sigma$ and pure white to σ linearly). Then the resulted 64×64 matrix is flattened to a vector \mathbf{f}_i . In the storage phase, $\sigma = 0.02$ was used to maintain the magnitude for \mathbf{f}_i and \mathbf{m}_i at an appropriate level. Reconstructing the image from the vector can be done by performing the procedure in reverse order.

The storage phase was proceeded for 40 seconds with the integration step size $\Delta t = 0.1$ and $\xi_i = \frac{\pi}{5}(i-1)$ (5-evenly sequenced points on $[0, \pi]$). The used parameters are $\omega = 1.5$, $\gamma = \rho = 0.5$, and $\tau = \frac{\pi}{3}$, respectively. Stable convergence of connectivity to \mathbf{W}^* is well achieved, when the initial condition $\mathbf{x}([- \tau \ 0])$ and $\mathbf{W}(0)$ are appropriately small.

The retrieval phase was proceeded for 15 seconds with $\Delta t = 0.01$ for appropriately small $\mathbf{x}(0)$. In Fig. 3, 4, and 5, the brightness threshold σ was adjusted to 0.005 for clear visibility, since the magnitude of the retrieved images are relatively small compared to original ones. Thus, any element of $\mathbf{x} \cdot \mathbf{r}_i$ having value outside $[-0.005 \ 0.005]$ is developed to a pixel of just pure black or white.

For the second memory task of composite group structures, the retrieval was proceeded for 15 seconds with $\Delta t = 0.01$ for appropriately small $\mathbf{x}(0)$. Multiple cues such as **John**_S + **Mary**_O in Fig. 8d are implemented by assigning each cue to its original sampling time through a harmonic pulse. In other words, the combined cue **John**_S + **Mary**_O is implemented as $\mathbf{b}_c(t) = \sin(\omega t - \xi_1)(\mathbf{f}_2 \otimes \mathbf{r}_1) + \sin(\omega t - \xi_3)(\mathbf{f}_1 \otimes \mathbf{r}_3)$.

References

- [1] K. I. Blum and L. F. Abbott, “A model of spatial map formation in the hippocampus of the rat,” *Neural computation*, vol. 8, no. 1, pp. 85–93, 1996.
- [2] R. P. Rao and T. J. Sejnowski, “Spike-timing-dependent hebbian plasticity as temporal difference learning,” *Neural computation*, vol. 13, no. 10, pp. 2221–2237, 2001.
- [3] M. Tsodyks, “Spike-timing-dependent synaptic plasticity—the long road towards understanding neuronal mechanisms of learning and memory,” *Trends in neurosciences*, vol. 25, no. 12, pp. 599–600, 2002.
- [4] B. Szatmáry and E. M. Izhikevich, “Spike-timing theory of working memory,” *PLoS Comput Biol*, vol. 6, no. 8, p. e1000879, 2010.

*Source for simplified MATLAB programs performing two numerical tests presented in this article can be found in the following link: <https://github.com/hkyoon94/NRSTDP.git>

- [5] J.-H. Han, S. A. Kushner, A. P. Yiu, H.-L. L. Hsiang, T. Buch, A. Waisman, B. Bontempi, R. L. Neve, P. W. Frankland, and S. A. Josselyn, “Selective erasure of a fear memory,” *Science*, vol. 323, no. 5920, pp. 1492–1496, 2009.
- [6] S. Ramirez, X. Liu, P.-A. Lin, J. Suh, M. Pignatelli, R. L. Redondo, T. J. Ryan, and S. Tonegawa, “Creating a false memory in the hippocampus,” *Science*, vol. 341, no. 6144, pp. 387–391, 2013.
- [7] R. L. Redondo, J. Kim, A. L. Arons, S. Ramirez, X. Liu, and S. Tonegawa, “Bidirectional switch of the valence associated with a hippocampal contextual memory engram,” *Nature*, vol. 513, no. 7518, pp. 426–430, 2014.
- [8] J. S. Kelso, *Dynamic patterns: The self-organization of brain and behavior*. MIT press, 1995.
- [9] G. G. Globus, *The postmodern brain*. J. Benjamins Publishing Company, 1995.
- [10] M. Breakspear, “Dynamic models of large-scale brain activity,” *Nature neuroscience*, vol. 20, no. 3, pp. 340–352, 2017.
- [11] T. J. Wills, C. Lever, F. Cacucci, N. Burgess, and J. O’Keefe, “Attractor dynamics in the hippocampal representation of the local environment,” *Science*, vol. 308, no. 5723, pp. 873–876, 2005.
- [12] E. T. Rolls, “An attractor network in the hippocampus: theory and neurophysiology,” *Learning & memory*, vol. 14, no. 11, pp. 714–731, 2007.
- [13] M. Tsodyks, “Attractor neural network models of spatial maps in hippocampus,” *Hippocampus*, vol. 9, no. 4, pp. 481–489, 1999.
- [14] S. Stringer, E. Rolls, and T. Trappenberg, “Self-organizing continuous attractor network models of hippocampal spatial view cells,” *Neurobiology of learning and memory*, vol. 83, no. 1, pp. 79–92, 2005.
- [15] C. Rennó-Costa, J. E. Lisman, and P. F. Verschure, “A signature of attractor dynamics in the ca3 region of the hippocampus,” *PLoS Comput Biol*, vol. 10, no. 5, p. e1003641, 2014.
- [16] E. T. Rolls, “Attractor networks,” *Wiley Interdisciplinary Reviews: Cognitive Science*, vol. 1, no. 1, pp. 119–134, 2010.
- [17] M. Tsanov and D. Manahan-Vaughan, “Long-term plasticity is proportional to theta-activity,” *PLoS One*, vol. 4, no. 6, p. e5850, 2009.
- [18] B. C. Lega, J. Jacobs, and M. Kahana, “Human hippocampal theta oscillations and the formation of episodic memories,” *Hippocampus*, vol. 22, no. 4, pp. 748–761, 2012.
- [19] W. Singer, “Neuronal synchrony: a versatile code for the definition of relations?,” *Neuron*, vol. 24, no. 1, pp. 49–65, 1999.
- [20] G. Buzsáki and A. Draguhn, “Neuronal oscillations in cortical networks,” *science*, vol. 304, no. 5679, pp. 1926–1929, 2004.

- [21] M. Siegel, M. R. Warden, and E. K. Miller, “Phase-dependent neuronal coding of objects in short-term memory,” *Proceedings of the National Academy of Sciences*, vol. 106, no. 50, pp. 21341–21346, 2009.
- [22] L. Susman, N. Brenner, and O. Barak, “Stable memory with unstable synapses,” *Nature communications*, vol. 10, no. 1, pp. 1–9, 2019.
- [23] P. Dayan, L. F. Abbott, *et al.*, “Theoretical neuroscience: computational and mathematical modeling of neural systems,” *Journal of Cognitive Neuroscience*, vol. 15, no. 1, pp. 154–155, 2003.
- [24] R. Kempter, W. Gerstner, and J. L. Van Hemmen, “Hebbian learning and spiking neurons,” *Physical Review E*, vol. 59, no. 4, p. 4498, 1999.
- [25] W. Singer and C. M. Gray, “Visual feature integration and the temporal correlation hypothesis,” *Annual review of neuroscience*, vol. 18, no. 1, pp. 555–586, 1995.
- [26] N. Gupta, S. S. Singh, and M. Stopfer, “Oscillatory integration windows in neurons,” *Nature communications*, vol. 7, no. 1, pp. 1–10, 2016.
- [27] U. Rutishauser, I. B. Ross, A. N. Mamelak, and E. M. Schuman, “Human memory strength is predicted by theta-frequency phase-locking of single neurons,” *Nature*, vol. 464, no. 7290, pp. 903–907, 2010.
- [28] D. L. Hintzman, “Minerva 2: A simulation model of human memory,” *Behavior Research Methods, Instruments, & Computers*, vol. 16, no. 2, pp. 96–101, 1984.
- [29] P. Kanerva, *Sparse distributed memory*. MIT press, 1988.
- [30] M. S. Humphreys, J. D. Bain, and R. Pike, “Different ways to cue a coherent memory system: A theory for episodic, semantic, and procedural tasks,” *Psychological Review*, vol. 96, no. 2, p. 208, 1989.
- [31] P. Smolensky, “Tensor product variable binding and the representation of symbolic structures in connectionist systems,” *Artificial intelligence*, vol. 46, no. 1-2, pp. 159–216, 1990.
- [32] J. B. Pollack, “Recursive distributed representations,” *Artificial Intelligence*, vol. 46, no. 1-2, pp. 77–105, 1990.

Supplementary Materials for: Neurodynamical Role of STDP in Storage and Retrieval of Associative Information

Hongkyu Yoon and Pilwon Kim

Department of Mathematical Sciences

Ulsan National Institute of Science and Technology(UNIST)

Ulsan Metropolitan City

44919, Republic of Korea

January 22, 2022

Contents

S1	Derivation of the Synaptic Evolution Equation	2
S2	Proofs for Full Theoretical Results and Lemmas	3
S3	Stability Analysis of Steady Synaptic Solution via Computation of Maximal Lyapunov Exponents	15

List of Figures

1	Graphical illustration of the types of retrieval cue component \mathbf{m}_c	10
2	Plot of numerically estimated maximal Lyapunov exponent of steady state solution of \mathbf{W} in storage phase	18

List of Tables

1	Values of memory plane's maximum average storage performance $\frac{1}{n} \sum_{i=1}^n \cos \theta_i$ for some $n (\geq 2)$	14
---	---	----

S1 Derivation of the Synaptic Evolution Equation

This section contains the derivation of the evolution equation of \mathbf{W} in the main text. As mentioned in the main text, the rate of change for each component of \mathbf{W} for firing rate networks is as the following:

$$\begin{aligned} \dot{W}_{ij}(t) = & -\gamma W_{ij}(t) + \underbrace{\rho \left(\int_0^\infty K(s) \phi(x_j(t-s)) \phi(x_i(t)) \, ds \right)}_{\text{pre-synaptic STDP}} \\ & + \underbrace{\rho \left(\int_{-\infty}^0 K(s) \phi(x_i(t+s)) \phi(x_j(t)) \, ds \right)}_{\text{post-synaptic STDP}}, \end{aligned} \quad (1)$$

where $\gamma > 0$ is a rate of decaying homeostatic plasticity, ρ a learning rate and $K : \mathbb{R} \rightarrow \mathbb{R}$ is a kernel describing the topology of STDP. Note that each bracketed term has a form of unnormalized convolution with each positive and negative domain of K . Thus, the characteristics of $K(s)$ describes the weight distribution for the time difference between pre and post-synaptic firing mirrored into STDP. The first term of integral describes the synaptic rate of change relevant to the situation when the pre-synaptic fire is *faster* than post-synaptic fire (written as ‘pre-synaptic STDP’ above), and for the second term, vice versa (‘post-synaptic STDP’). If $K(s)$ is perfectly anti-symmetric (i.e., $a_P = a_D$ and $\tau_P = \tau_D$), then the effect of both positive and negative synaptic plasticity will be purely anti-symmetric.

Physically $K(s)$ is conventionally modeled to decay to 0 as $s \rightarrow \pm\infty$, and to reach maximum near origin. However, main article only considered the case with more simplified kernel $K(s)$ with shape

$$K(s) := \begin{cases} \delta(s - s_0) & s > 0 \\ -\delta(s + s_0) & s \leq 0, \end{cases} \quad (2)$$

where $\delta(\cdot)$ represents a Dirac-delta function with $s_0 > 0$, being anti-symmetric. This represents simplified STDP mechanism based on Hebbian paradigm, with *synaptic delay* (communication time) τ introduced.

Since convolution of any $f : \mathbb{R} \rightarrow \mathbb{R}$ with Dirac-delta function $\delta(s - s_0)$ on any domain $\Omega \subset \mathbb{R}$ with $s_0 \in \Omega$ yields $f(s_0)$, i.e., $\int_\Omega \delta(s - s_0) f(s) \, ds = f(s_0)$, so Eq. (1) with such type of kernel becomes

$$\dot{W}_{ij}(t) = -\gamma W_{ij}(t) + \rho (\phi(x_j(t - s_0)) \phi(x_i(t)) - \phi(x_i(t - s_0)) \phi(x_j(t))). \quad (3)$$

Rewriting it in matrix form,

$$\dot{\mathbf{W}}(t) = -\gamma \mathbf{W}(t) + \rho (\phi(\mathbf{x}(t)) \phi(\mathbf{x}(t - s_0))^\top - \phi(\mathbf{x}(t - s_0)) \phi(\mathbf{x}(t))^\top). \quad (4)$$

Now, specifying s_0 as $s_0 = \tau$ (synaptic communication time), applying low level activity approximation $\phi(x) \approx x$, and introducing notation $\mathbf{x}_\tau = \mathbf{x}(t - \tau)$ indicating the τ -delayed term of $\mathbf{x}(t)$ as in the main text, then Eq. (4) becomes

$$\dot{\mathbf{W}} = -\gamma \mathbf{W} + \rho (\mathbf{x} \mathbf{x}_\tau^\top - \mathbf{x}_\tau \mathbf{x}^\top), \quad (5)$$

obtaining our equation on $\dot{\mathbf{W}}$. Here, the term $-\gamma \mathbf{W}$ acts as homeostatic decay and $\rho(\mathbf{x} \mathbf{x}_\tau^\top - \mathbf{x}_\tau \mathbf{x}^\top)$ acts as actual learning operator by STDP.

S2 Proofs for Full Theoretical Results and Lemmas

In this section, we give full statements and detailed proofs for each mathematical results and important theorems abbreviated in the main text. In order to begin the proofs of full main theorems, we introduce two following preliminary lemmas.

This first lemma shows the fact that the input of the form of harmonic pulse ensemble in the main text lies in some 2-dimensional plane in the neural state space.

Lemma A. *Let $\mathbf{m}_i \in \mathbb{R}^N$, $\xi_i \in \mathbb{R}$ with $i = 1, \dots, n$, and $\omega \in \mathbb{R} \setminus \{0\}$. Then, the trajectory of following time-dependent function*

$$\mathbf{b}(t) = \sum_{i=1}^n \sin(\omega t - \xi_i) \mathbf{m}_i \quad (6)$$

is periodic and embedded in some 2-dimensional plane $\text{Span}\{\mathbf{u}, \mathbf{v}\}$ in the state space where vectors $\mathbf{u}, \mathbf{v} \in \mathbb{R}^N$ are defined as

$$\begin{cases} \mathbf{u} = -\Psi \sin \boldsymbol{\xi} \\ \mathbf{v} = \Psi \cos \boldsymbol{\xi}, \end{cases} \quad (7)$$

where $\Psi = [\mathbf{m}_1 | \mathbf{m}_2 | \dots | \mathbf{m}_n] \in \mathbb{R}^{N \times n}$, $\sin \boldsymbol{\xi} = [\sin \xi_1 \ \sin \xi_2 \ \dots \ \sin \xi_n]^\top \in \mathbb{R}^n$, and $\cos \boldsymbol{\xi} = [\cos \xi_1 \ \cos \xi_2 \ \dots \ \cos \xi_n]^\top \in \mathbb{R}^n$.

Proof. Note that element-wisely, $\mathbf{b}(t) = [b_1(t) \ b_2(t) \ \dots \ b_N(t)]^\top$ satisfies

$$b_j(t) = \sum_{i=1}^n m_{i,j} \sin(\omega t - \xi_i), \quad j = 1, \dots, N, \quad (8)$$

where $\mathbf{m}_i = [m_{i,1} \ m_{i,2} \ \dots \ m_{i,N}]^\top$. Now, observe

$$\begin{aligned} b_j(t) &= \sum_{i=1}^n m_{i,j} (\sin \omega t \cos \xi_i - \cos \omega t \sin \xi_i) \\ &= \cos \omega t \left(\sum_i m_{i,j} (-\sin \xi_i) \right) + \sin \omega t \left(\sum_i m_{i,j} \cos \xi_i \right), \quad j = 1, \dots, N. \end{aligned} \quad (9)$$

Thus if we introduce

$$\begin{cases} \mathbf{u} = -[\sum_{i=1}^n m_{i,1} \sin \xi_i \ \dots \ \sum_{i=1}^n m_{i,N} \sin \xi_i]^\top \\ \mathbf{v} = [\sum_{i=1}^n m_{i,1} \cos \xi_i \ \dots \ \sum_{i=1}^n m_{i,N} \cos \xi_i]^\top, \end{cases} \quad (10)$$

then this choice of \mathbf{u}, \mathbf{v} can be represented in alternate form of $\mathbf{u} = -\Psi \sin \boldsymbol{\xi}$ and $\mathbf{v} = \Psi \cos \boldsymbol{\xi}$ where Ψ , $\sin \boldsymbol{\xi}$, and $\cos \boldsymbol{\xi}$ are defined as in the statement, and guarantees

$$\mathbf{b}(t) = \cos \omega t \mathbf{u} + \sin \omega t \mathbf{v} \quad (11)$$

by (9). Therefore $\mathbf{b}(t)$ is periodic and embedded in plane $\text{Span}\{\mathbf{u}, \mathbf{v}\}$. \square

Next, the following second lemma is about some useful algebraic relations of frequently appearing periodic functions which describes the solution behavior of our model.

Lemma B. Let $c_{i,[\lambda,\omega]}(t)$ be the following periodic functions in t , with parameters $\lambda, \omega \in \mathbb{R}^+$, which is defined as

$$\begin{cases} c_{1,[\lambda,\omega]}(t) = \frac{1}{2} \left(\frac{\cos(\omega t - \theta_{-,[\lambda,\omega]})}{\sqrt{\Phi_{-,[\lambda,\omega]}}} + \frac{\cos(\omega t - \theta_{+,[\lambda,\omega]})}{\sqrt{\Phi_{+,[\lambda,\omega]}}} \right) \\ c_{2,[\lambda,\omega]}(t) = \frac{1}{2} \left(\frac{\sin(\omega t - \theta_{-,[\lambda,\omega]})}{\sqrt{\Phi_{-,[\lambda,\omega]}}} - \frac{\sin(\omega t - \theta_{+,[\lambda,\omega]})}{\sqrt{\Phi_{+,[\lambda,\omega]}}} \right) \\ c_{3,[\lambda,\omega]}(t) = \frac{1}{2} \left(\frac{\sin(\omega t - \theta_{-,[\lambda,\omega]})}{\sqrt{\Phi_{-,[\lambda,\omega]}}} + \frac{\sin(\omega t - \theta_{+,[\lambda,\omega]})}{\sqrt{\Phi_{+,[\lambda,\omega]}}} \right) \\ c_{4,[\lambda,\omega]}(t) = -\frac{1}{2} \left(\frac{\cos(\omega t - \theta_{-,[\lambda,\omega]})}{\sqrt{\Phi_{-,[\lambda,\omega]}}} + \frac{\cos(\omega t - \theta_{+,[\lambda,\omega]})}{\sqrt{\Phi_{+,[\lambda,\omega]}}} \right) \end{cases} \quad (12)$$

where $\theta_{\pm,[\lambda,\omega]} = \tan^{-1}(\omega \pm \lambda)$, $\Phi_{\pm,[\lambda,\omega]} = \lambda^2 \pm 2\omega\lambda + \omega^2 + 1$. Let's denote $\frac{d}{dt}c_{i,[\lambda,\omega]}(t)$ with $\dot{c}_{i,[\lambda,\omega]}(t)$. Then, the followings are true:

1. $\dot{c}_{1,[\lambda,\omega]} = -\omega c_{3,[\lambda,\omega]}$, $\dot{c}_{2,[\lambda,\omega]} = -\omega c_{4,[\lambda,\omega]}$, $\dot{c}_{3,[\lambda,\omega]} = \omega c_{1,[\lambda,\omega]}$, and $\dot{c}_{4,[\lambda,\omega]} = \omega c_{2,[\lambda,\omega]}$.
2.
 - a. $c_{1,[\lambda,\omega]}(t) - \omega c_{3,[\lambda,\omega]}(t) + \lambda c_{2,[\lambda,\omega]}(t) = \cos \omega t$.
 - b. $c_{1,[\lambda,\omega]}(t) + \omega c_{3,[\lambda,\omega]}(t) + \lambda c_{4,[\lambda,\omega]}(t) = \sin \omega t$.
 - c. $c_{2,[\lambda,\omega]}(t) - \omega c_{4,[\lambda,\omega]}(t) - \lambda c_{1,[\lambda,\omega]}(t) = 0$.
 - d. $c_{2,[\lambda,\omega]}(t) + \omega c_{4,[\lambda,\omega]}(t) - \lambda c_{3,[\lambda,\omega]}(t) = 0$.

Proof. Statement 1 can be straightforwardly shown by direct differentiation. For statement 2, omitting the $[\lambda,\omega]$ notations in $\theta_{\pm,[\lambda,\omega]}$, observe that

$$\begin{aligned} & c_{1,[\lambda,\omega]}(t) - \omega c_{3,[\lambda,\omega]}(t) + \lambda c_{2,[\lambda,\omega]}(t) \\ &= \frac{1}{2} \left(\frac{\cos(\omega t - \theta_-) - (\omega - \lambda) \sin(\omega t - \theta_-)}{\sqrt{\Phi_{-,[\lambda,\omega]}}} + \frac{\cos(\omega t - \theta_+) - (\omega + \lambda) \sin(\omega t - \theta_+)}{\sqrt{\Phi_{+,[\lambda,\omega]}}} \right) \end{aligned} \quad (13)$$

$$\begin{aligned} &= \frac{1}{2} \left(\frac{\sqrt{\Phi_{-,[\lambda,\omega]}} \cos(\omega t - \theta_- + \theta_-) + \sqrt{\Phi_{+,[\lambda,\omega]}} \cos(\omega t - \theta_+ + \theta_+)}{\sqrt{\Phi_{-,[\lambda,\omega]}}} \right) \\ &= \cos \omega t, \end{aligned} \quad (14)$$

where Eq. (13) comes from direct substitution and Eq. (14) comes from the fact $1^2 + (\omega \pm \lambda)^2 = \Phi_{\pm,[\lambda,\omega]}$ and $a \cos t - b \sin t = \sqrt{a^2 + b^2} \cos(t + \phi)$ with $\phi = -\tan^{-1}(a/b)$, so 2a has been shown. Differentiating both sides of this result respect to t using statement 1 directly yields $c_{1,[\lambda,\omega]}(t) + \omega c_{3,[\lambda,\omega]}(t) + \lambda c_{4,[\lambda,\omega]}(t) = \sin \omega t$, which is 2b. Similarly, one can also check 2c by

$$\begin{aligned} & c_{2,[\lambda,\omega]}(t) - \omega c_{4,[\lambda,\omega]}(t) - \lambda c_{1,[\lambda,\omega]}(t) \\ &= \frac{1}{2} \left(\frac{\sin(\omega t - \theta_-) + (\omega - \lambda) \cos(\omega t - \theta_-)}{\sqrt{\Phi_{-,[\lambda,\omega]}}} - \frac{\sin(\omega t - \theta_+) + (\omega + \lambda) \cos(\omega t - \theta_+)}{\sqrt{\Phi_{+,[\lambda,\omega]}}} \right) \\ &= \frac{1}{2} \left(\frac{\sqrt{\Phi_{-,[\lambda,\omega]}} \sin(\omega t - \theta_- + \theta_-) - \sqrt{\Phi_{+,[\lambda,\omega]}} \sin(\omega t - \theta_+ + \theta_+)}{\sqrt{\Phi_{-,[\lambda,\omega]}}} \right) \\ &= 0, \end{aligned} \quad (15)$$

and differentiating both sides of this result respect to t using statement 1 also yields $c_{2,[\lambda,\omega]}(t) + \omega c_{4,[\lambda,\omega]}(t) - \lambda c_{3,[\lambda,\omega]}(t) = 0$, which is statement 2d. \square

Now, we are ready to present our main theorems: the following is a complete version of Theorem 1 from main text describing the existence of steady synaptic solution of storage phase.

Theorem 1. (STEADY SYNAPTIC SOLUTION) *Consider system*

$$\begin{cases} \dot{\mathbf{x}} = -\mathbf{x} + \mathbf{W}\mathbf{x} + \mathbf{b}(t) \\ \dot{\mathbf{W}} = -\gamma\mathbf{W} + \rho(\mathbf{x}\mathbf{x}^\top - \mathbf{x}_\tau\mathbf{x}_\tau^\top), \end{cases} \quad (16)$$

with $\mathbf{x} \in \mathbb{R}^N$, $\mathbf{W} \in \mathbb{R}^{N \times N}$, and $\mathbf{b}(t) \in \mathbb{R}^N$ being the continued external input with form

$$\mathbf{b}(t) = \sum_{i=1}^n \sin(\omega t - \xi_i) \mathbf{m}_i \quad (17)$$

where $\{\mathbf{m}_1, \mathbf{m}_2, \dots, \mathbf{m}_n\}$ is a linearly independent set with $\mathbf{m}_i \in \mathbb{R}^N$ (not necessarily normalized) and $\omega \in \mathbb{R} \setminus \{0\}$, $\xi_i \in \mathbb{R}$ being arbitrary constants. Then, there exists a steady state solution \mathbf{W}^* of \mathbf{W} and a periodic solution $\mathbf{x}^*(t)$ of \mathbf{x} for (16), such that

$$\begin{cases} \mathbf{W}^* = \alpha(\mathbf{v}\mathbf{u}^\top - \mathbf{u}\mathbf{v}^\top) \\ \mathbf{x}^*(t) = f(t)\mathbf{u} + g(t)\mathbf{v} \end{cases} \quad (18)$$

where $\alpha \in \mathbb{R}$, and $f, g : \mathbb{R} \rightarrow \mathbb{R}$ periodic functions.

Proof. Let $c_{i,[\lambda,\omega]}(t)$ and $\Phi_{\pm,[\lambda,\omega]}$ be the periodic functions with parameters λ, ω and polynomials in λ defined as in lemma B respectively. Point-blank, we propose the followings: Vectors \mathbf{u}, \mathbf{v} are given as a form in lemma A (i.e., $\mathbf{u} = -\Psi \sin \xi$, $\mathbf{v} = \Psi \cos \xi$), and $\alpha, f(t)$ and $g(t)$ are given by

$$\begin{cases} \alpha = \frac{\lambda_0}{\eta_1 \eta_2 \sqrt{1 - \mu^2}} \\ f(t) = c_{1,[\lambda_0,\omega]}(t) - \frac{\mu}{\sqrt{1 - \mu^2}} c_{2,[\lambda_0,\omega]}(t) - \frac{\eta_2}{\eta_1 \sqrt{1 - \mu^2}} c_{4,[\lambda_0,\omega]}(t) \\ g(t) = c_{3,[\lambda_0,\omega]}(t) + \frac{\mu}{\sqrt{1 - \mu^2}} c_{4,[\lambda_0,\omega]}(t) + \frac{\eta_1}{\eta_2 \sqrt{1 - \mu^2}} c_{2,[\lambda_0,\omega]}(t) \end{cases} \quad (19)$$

where λ_0 is a real root* of algebraic equation $h(\lambda) = 0$ with

$$h(\lambda) = \frac{\lambda \Phi_{-,[\lambda,\omega]} \Phi_{+,[\lambda,\omega]}}{(\eta_1 \eta_2 \sqrt{1 - \mu^2}) (\lambda^2 + \omega^2 + 1) + (\eta_1^2 + \eta_2^2) \omega \lambda} - \frac{\rho \sin \omega \tau}{\gamma}, \quad (20)$$

and constants η_1, η_2 , and μ are

$$\eta_1 = \|\mathbf{u}\|, \eta_2 = \|\mathbf{v}\|, \text{ and } \mu = \frac{\mathbf{u}^\top \mathbf{v}}{\|\mathbf{u}\| \|\mathbf{v}\|}. \quad (21)$$

To begin with, we will show that $(\mathbf{x}^*(t), \mathbf{W}^*)$ in Eq. (18) with condition (19), (20), and (21) satisfies Eq. (16). First, let's start with showing $\dot{\mathbf{x}}^* + \mathbf{x}^* - \mathbf{W}^* \mathbf{x}^* = \mathbf{b}(t)$. According to lemma A, such $\mathbf{b}(t)$ of form (17) is equivalent with $\cos \omega t \mathbf{u} + \sin \omega t \mathbf{v}$ on plane (see Eq. (11)), so it only requires checking $\dot{\mathbf{x}}^* + \mathbf{x}^* - \mathbf{W}^* \mathbf{x}^* = \cos \omega t \mathbf{u} + \sin \omega t \mathbf{v}$. To do this, from lemma B-1, firstly see that $\dot{c}_{1,[\lambda_0,\omega]} = -\omega c_{3,[\lambda_0,\omega]}$, $\dot{c}_{2,[\lambda_0,\omega]} = -\omega c_{4,[\lambda_0,\omega]}$, $\dot{c}_{3,[\lambda_0,\omega]} = \omega c_{1,[\lambda_0,\omega]}$, and $\dot{c}_{4,[\lambda_0,\omega]} = \omega c_{2,[\lambda_0,\omega]}$. Thus from complete expression of $\mathbf{x}^*(t)$,

Here, the value of λ_0 tends to be maximized when the value $-\frac{\rho \sin \omega \tau}{\gamma}$ is minimized. This is the reason for choosing $\tau = \frac{\pi}{3} = \frac{\pi}{2\omega}$ in the main text, in order to acquire the highest norm of converging connectivity \mathbf{W}^ . If the real λ_0 satisfying $h(\lambda_0) = 0$ is unique, then the solution pair $(\mathbf{x}^*(t), \mathbf{W}^*)$ is unique.

$$\begin{aligned}\dot{\mathbf{x}}^*(t) + \mathbf{x}^*(t) = & \left((c_1 - \omega c_3) + \frac{\mu}{\sqrt{1-\mu^2}}(-c_2 + \omega c_4) + \frac{\eta_2}{\eta_1 \sqrt{1-\mu^2}}(-c_2 - \omega c_4) \right) \mathbf{u} \\ & + \left((c_1 + \omega c_3) + \frac{\mu}{\sqrt{1-\mu^2}}(c_2 + \omega c_4) + \frac{\eta_1}{\eta_2 \sqrt{1-\mu^2}}(c_2 - \omega c_4) \right) \mathbf{v},\end{aligned}\quad (22)$$

where $[\lambda_0, \omega]$ notations in $c_{i, [\lambda_0, \omega]}$ are omitted.

On the other hand, for remaining computations, we introduce some additional definitions in order to make the following processes concise. Set \mathbf{u}_\perp and \mathbf{v}_\perp as

$$\mathbf{u}_\perp = \frac{1}{\sqrt{1-\mu^2}} \left(-\mu \mathbf{u} + \frac{\eta_1}{\eta_2} \mathbf{v} \right), \quad \mathbf{v}_\perp = \frac{1}{\sqrt{1-\mu^2}} \left(-\frac{\eta_2}{\eta_1} \mathbf{u} + \mu \mathbf{v} \right), \quad (23)$$

where $\eta_1 = \|\mathbf{u}\|$, $\eta_2 = \|\mathbf{v}\|$ and $\mu = \mathbf{u}^\top \mathbf{v} / (\|\mathbf{u}\| \|\mathbf{v}\|)$. Then one can see that $\mathbf{u}_\perp \perp \mathbf{u}$ satisfying $\|\mathbf{u}_\perp\| = \|\mathbf{u}\|$ and $\mathbf{v}_\perp \perp \mathbf{v}$ satisfying $\|\mathbf{v}_\perp\| = \|\mathbf{v}\|$, and can further check that the expression for $\mathbf{x}^*(t)$ is equivalent with $c_{1, [\lambda_0, \omega]}(t)\mathbf{u} + c_{2, [\lambda_0, \omega]}(t)\mathbf{u}_\perp + c_{3, [\lambda_0, \omega]}(t)\mathbf{v} + c_{4, [\lambda_0, \omega]}(t)\mathbf{v}_\perp$. Now performing computation of $\mathbf{W}^* \mathbf{x}^*(t)$ yields

$$\begin{aligned}\mathbf{W}^* \mathbf{x}^*(t) &= \frac{\lambda_0}{\eta_1 \eta_2 \sqrt{1-\mu^2}} (\mathbf{v} \mathbf{u}^\top - \mathbf{u} \mathbf{v}^\top) (c_{1, [\lambda_0, \omega]} \mathbf{u} + c_{2, [\lambda_0, \omega]} \mathbf{u}_\perp + c_{3, [\lambda_0, \omega]} \mathbf{v} + c_{4, [\lambda_0, \omega]} \mathbf{v}_\perp) \\ &= \frac{\lambda_0}{\eta_1 \eta_2 \sqrt{1-\mu^2}} \left((\eta_1^2 c_{1, [\lambda_0, \omega]} + \eta_1 \eta_2 \mu c_{3, [\lambda_0, \omega]} - \eta_1 \eta_2 \sqrt{1-\mu^2} c_{4, [\lambda_0, \omega]}) \mathbf{v} \right. \\ &\quad \left. + (-\eta_1 \eta_2 \mu c_{1, [\lambda_0, \omega]} - \eta_1 \eta_2 \sqrt{1-\mu^2} c_{2, [\lambda_0, \omega]} - \eta_2 c_{3, [\lambda_0, \omega]}) \mathbf{u} \right) \\ &= -\lambda_0 \left(c_{2, [\lambda_0, \omega]} + \frac{\mu}{\sqrt{1-\mu^2}} c_{1, [\lambda_0, \omega]} + \frac{\eta_2}{\eta_1 \sqrt{1-\mu^2}} c_{3, [\lambda_0, \omega]} \right) \mathbf{u} \\ &\quad + \lambda_0 \left(-c_{4, [\lambda_0, \omega]} + \frac{\mu}{\sqrt{1-\mu^2}} c_{3, [\lambda_0, \omega]} + \frac{\eta_1}{\eta_2 \sqrt{1-\mu^2}} c_{1, [\lambda_0, \omega]} \right) \mathbf{v},\end{aligned}\quad (24)$$

where we used the facts $\mathbf{u}^\top \mathbf{u} = \eta_1^2$, $\mathbf{v}^\top \mathbf{v} = \eta_2^2$, $\mathbf{u}^\top \mathbf{v} = \eta_1 \eta_2 \mu$, $\mathbf{u}^\top \mathbf{v}_\perp = -\eta_1 \eta_2 \sqrt{1-\mu^2}$, and $\mathbf{v}^\top \mathbf{u}_\perp = \eta_1 \eta_2 \sqrt{1-\mu^2}$. Now combining above results with full notations, we have

$$\begin{aligned}\dot{\mathbf{x}}^*(t) + \mathbf{x}^*(t) - \mathbf{W}^* \mathbf{x}^*(t) &= \left((c_{1, [\lambda_0, \omega]} - \omega c_{3, [\lambda_0, \omega]} + \lambda_0 c_{2, [\lambda_0, \omega]}) - (c_{2, [\lambda_0, \omega]} - \omega c_{4, [\lambda_0, \omega]} - \lambda_0 c_{1, [\lambda_0, \omega]}) \frac{\mu}{\sqrt{1-\mu^2}} \right. \\ &\quad \left. - (c_{2, [\lambda_0, \omega]} + \omega c_{4, [\lambda_0, \omega]} - \lambda_0 c_{3, [\lambda_0, \omega]}) \frac{\eta_2}{\eta_1 \sqrt{1-\mu^2}} \right) \mathbf{u}\end{aligned}\quad (25)$$

$$\begin{aligned}& + \left((c_{1, [\lambda_0, \omega]} + \omega c_{3, [\lambda_0, \omega]} + \lambda_0 c_{4, [\lambda_0, \omega]}) + (c_{2, [\lambda_0, \omega]} + \omega c_{4, [\lambda_0, \omega]} - \lambda_0 c_{3, [\lambda_0, \omega]}) \frac{\mu}{\sqrt{1-\mu^2}} \right. \\ &\quad \left. + (c_{2, [\lambda_0, \omega]} - \omega c_{4, [\lambda_0, \omega]} - \lambda_0 c_{1, [\lambda_0, \omega]}) \frac{\eta_1}{\eta_2 \sqrt{1-\mu^2}} \right) \mathbf{v}.\end{aligned}\quad (26)$$

Now, lemma B-2a, 2c, and 2d tells us that each three coefficients in terms of $c_{i, [\lambda_0, \omega]}(t)$ of (25) in RHS is $\cos \omega t$, 0, and 0 respectively, thus simplified only into $\cos \omega t \mathbf{u}$. Similarly, each three coefficients

in terms of $c_{i,[\lambda_0,\omega]}(t)$ in (26) becomes $\sin \omega t$, 0, and 0 by lemma B-2b, 2c, and 2d respectively, thus yielding $\sin \omega t \mathbf{v}$. Therefore in total, completing the proof of $\dot{\mathbf{x}}^*(t) + \mathbf{x}^*(t) - \mathbf{W}^* \mathbf{x}^*(t) = \cos \omega t \mathbf{u} + \sin \omega t \mathbf{v} = \mathbf{b}(t)$.

Now, it remains to confirm $-\gamma \mathbf{W}^* + \rho(\mathbf{x}^* \mathbf{x}_\tau^{*\top} - \mathbf{x}_\tau^* \mathbf{x}^{*\top}) = \mathbf{O}$. In order to show this, first we have to compute the term $\mathbf{x}^* \mathbf{x}_\tau^{*\top} - \mathbf{x}_\tau^* \mathbf{x}^{*\top}$. With the help of trigonometric relations

$$\begin{cases} \cos(\omega t - \theta_-) \sin(\omega(t - \tau) - \theta_+) - \cos(\omega(t - \tau) - \theta_-) \sin(\omega t - \theta_+) = -\sin \omega \tau \cos(\theta_- - \theta_+) \\ \sin(\omega t - \theta_-) \sin(\omega(t - \tau) - \theta_+) - \sin(\omega(t - \tau) - \theta_-) \sin(\omega t - \theta_+) = \sin \omega \tau \sin(\theta_- - \theta_+) \\ \sin(\omega t - \theta_-) \cos(\omega(t - \tau) - \theta_+) - \sin(\omega(t - \tau) - \theta_-) \cos(\omega t - \theta_+) = \sin \omega \tau \cos(\theta_- - \theta_+) \\ \cos(\omega t - \theta_-) \cos(\omega(t - \tau) - \theta_+) - \cos(\omega(t - \tau) - \theta_-) \cos(\omega t - \theta_+) = \sin \omega \tau \sin(\theta_- - \theta_+) \end{cases} \quad (27)$$

and after some lengthy computations, we get

$$\begin{aligned} & \mathbf{x}^*(t) \mathbf{x}^*(t - \tau)^\top - \mathbf{x}^*(t - \tau) \mathbf{x}^*(t)^\top \\ &= \frac{\sin \omega \tau}{4} \left[\left(\frac{1}{\Phi_{-,[\lambda_0,\omega]}} - \frac{1}{\Phi_{+,[\lambda_0,\omega]}} \right) ((\mathbf{u}_\perp \mathbf{u}^\top - \mathbf{u} \mathbf{u}_\perp^\top) + (\mathbf{v}_\perp \mathbf{v}^\top - \mathbf{v} \mathbf{v}_\perp^\top)) \right. \\ & \quad + \left(\frac{1}{\Phi_{-,[\lambda_0,\omega]}} + \frac{1}{\Phi_{+,[\lambda_0,\omega]}} + \frac{2 \cos(\theta_{-,[\lambda_0,\omega]} - \theta_{+,[\lambda_0,\omega]})}{\Phi_{-,[\lambda_0,\omega]} \Phi_{+,[\lambda_0,\omega]}} \right) (\mathbf{v} \mathbf{u}^\top - \mathbf{u} \mathbf{v}^\top) \\ & \quad + \left(\frac{1}{\Phi_{-,[\lambda_0,\omega]}} + \frac{1}{\Phi_{+,[\lambda_0,\omega]}} - \frac{2 \cos(\theta_{-,[\lambda_0,\omega]} - \theta_{+,[\lambda_0,\omega]})}{\Phi_{-,[\lambda_0,\omega]} \Phi_{+,[\lambda_0,\omega]}} \right) (\mathbf{v}_\perp \mathbf{u}_\perp^\top - \mathbf{u}_\perp \mathbf{v}_\perp^\top) \\ & \quad \left. + \frac{2 \sin(\theta_{-,[\lambda_0,\omega]} - \theta_{+,[\lambda_0,\omega]})}{\Phi_{-,[\lambda_0,\omega]} \Phi_{+,[\lambda_0,\omega]}} ((\mathbf{v}_\perp \mathbf{u}^\top - \mathbf{u} \mathbf{v}_\perp^\top) + (\mathbf{v} \mathbf{u}_\perp^\top - \mathbf{u}_\perp \mathbf{v}^\top)) \right], \end{aligned} \quad (28)$$

which is a constant in t as expected. Here, from (23), one can easily check that the six anti-symmetric matrix terms in (28) have the following relations:

$$\begin{cases} \mathbf{u}_\perp \mathbf{u}^\top - \mathbf{u} \mathbf{u}_\perp^\top = \frac{\eta_1}{\eta_2 \sqrt{1 - \mu^2}} (\mathbf{v} \mathbf{u}^\top - \mathbf{u} \mathbf{v}^\top) \\ \mathbf{v}_\perp \mathbf{v}^\top - \mathbf{v} \mathbf{v}_\perp^\top = \frac{\eta_2}{\eta_1 \sqrt{1 - \mu^2}} (\mathbf{v} \mathbf{u}^\top - \mathbf{u} \mathbf{v}^\top) \\ \mathbf{v}_\perp \mathbf{u}_\perp^\top - \mathbf{u}_\perp \mathbf{v}_\perp^\top = \mathbf{v} \mathbf{u}^\top - \mathbf{u} \mathbf{v}^\top \\ \mathbf{v} \mathbf{u}_\perp^\top - \mathbf{u}_\perp \mathbf{v}^\top = -(\mathbf{v}_\perp \mathbf{u}^\top - \mathbf{u} \mathbf{v}_\perp^\top). \end{cases} \quad (29)$$

Now simplifying (28) using (29) in terms of $\mathbf{v} \mathbf{u}^\top - \mathbf{u} \mathbf{v}^\top$ and substituting the result into $-\gamma \mathbf{W}^* + \rho(\mathbf{x}^* \mathbf{x}_\tau^{*\top} - \mathbf{x}_\tau^* \mathbf{x}^{*\top})$ alongside substituting $\mathbf{W}^* = \lambda_0(\mathbf{v} \mathbf{u}^\top - \mathbf{u} \mathbf{v}^\top) / (\eta_1 \eta_2 \sqrt{1 - \mu^2})$ together, then

$$\begin{aligned} & -\gamma \mathbf{W}^* + \rho(\mathbf{x}^* \mathbf{x}_\tau^{*\top} - \mathbf{x}_\tau^* \mathbf{x}^{*\top}) \\ &= \left[-\frac{\gamma \lambda_0}{\eta_1 \eta_2 \sqrt{1 - \mu^2}} + \frac{\rho \sin \omega \tau}{\Phi_{-,[\lambda_0,\omega]} \Phi_{+,[\lambda_0,\omega]}} \left(\lambda_0^2 + \frac{(\eta_1^2 + \eta_2^2) \omega}{\eta_1 \eta_2 \sqrt{1 - \mu^2}} \lambda_0 + \omega^2 + 1 \right) \right] (\mathbf{v} \mathbf{u}^\top - \mathbf{u} \mathbf{v}^\top). \end{aligned} \quad (30)$$

Moreover, from the fact that λ_0 is a root of (20), we know

$$\frac{\lambda_0 \Phi_{-,[\lambda_0,\omega]} \Phi_{+,[\lambda_0,\omega]}}{(\eta_1 \eta_2 \sqrt{1 - \mu^2}) (\lambda_0^2 + \omega^2 + 1) + (\eta_1^2 + \eta_2^2) \omega \lambda_0} - \frac{\rho \sin \omega \tau}{\gamma} = 0, \quad (31)$$

and slight more algebra using this shows that the large-bracketed term in (30) turns out to be 0. So this proves $-\gamma \mathbf{W}^* + \rho(\mathbf{x}^* \mathbf{x}_\tau^{*\top} - \mathbf{x}_\tau^* \mathbf{x}^{*\top}) = \mathbf{O}$.

From all above, we conclude that (16) has a solution of form (18). \square

The following theorem is a complete version of Theorem 2 describing the perfect retrieval time in our model's retrieval phase from the main text. The version in the main text only corresponds to statement 1 and 2 of this theorem.

Theorem 2. (PERFECT RETRIEVAL) Consider a set $\{\mathbf{m}_1, \mathbf{m}_2, \dots, \mathbf{m}_n\}$ of linearly independent vectors $\mathbf{m}_i \in \mathbb{R}^N$ ($N \geq n$), and define a subspace \mathcal{M} of \mathbb{R}^N as, $\mathcal{M} = \text{Span}\{\mathbf{m}_1, \mathbf{m}_2, \dots, \mathbf{m}_n\}$. Let \mathbf{u}, \mathbf{v} be arbitrary linearly independent vectors in $\mathcal{M} \setminus \{\mathbf{0}\}$ and define a subspace S of \mathcal{M} as $S = \text{Span}\{\mathbf{u}, \mathbf{v}\}$. Now, let $\mathbf{x}_r(t)$ be the solution of equation

$$\dot{\mathbf{x}} = -\mathbf{x} + \mathbf{W}^* \mathbf{x} + \sin \omega t \mathbf{m}_c \quad (32)$$

where $\mathbf{W}^* = \alpha(\mathbf{v}\mathbf{u}^\top - \mathbf{u}\mathbf{v}^\top) \in \wedge^2(S)$ with $\alpha, \omega \in \mathbb{R} \setminus \{0\}$, and $\mathbf{m}_c \in \mathbb{R}^N \setminus \{\mathbf{0}\}$ given arbitrary. Then, $\mathbf{x}_r(t)$ asymptotically approaches to some periodic motion $\mathbf{x}_r^*(t)$, which is also a solution. Furthermore, defining $t^\dagger > 0$ as

$$t^\dagger = \frac{1}{\omega} \tan^{-1} \omega \mod \frac{\pi}{\omega}, \quad (33)$$

then the followings are also true:

1. If $\mathbf{m}_c \in S_\perp^c \cap \mathcal{M}^c$, then only for $t = t^\dagger$, $\mathbf{x}_r^*(t) \in \mathcal{M} \setminus \{\mathbf{0}\}$ and in fact $\mathbf{x}_r^*(t^\dagger) \in S$.
2. If $\mathbf{m}_c \in S_\perp^c \cap \mathcal{M}$, then $\forall t > 0$, $\mathbf{x}_r^*(t) \in \mathcal{M} \setminus \{\mathbf{0}\}$, and in fact $\mathbf{x}_r^*(t^\dagger) \in S$.
3. If $\mathbf{m}_c \in S_\perp \cap \mathcal{M}^c$, then $\forall t > 0$, $\mathbf{x}_r^*(t) \notin \mathcal{M} \setminus \{\mathbf{0}\}$ and in fact $\mathbf{x}_r^*(t^\dagger) = \mathbf{0}$.
4. If $\mathbf{m}_c \in S_\perp \cap \mathcal{M}$, then $\forall t > 0$ except $t = t^\dagger$, $\mathbf{x}_r^*(t) \in \mathcal{M} \setminus \{\mathbf{0}\}$, and in fact $\mathbf{x}_r^*(t^\dagger) = \mathbf{0}$.

Proof. Since Eq. (32) is a perturbed linear ordinary differential equation, we can obtain explicit solution of $\mathbf{x}_r(t)$ using the variational formula, i.e.,

$$\begin{aligned} \mathbf{x}_r(t) &= e^{t(\mathbf{W}^* - \mathbf{I})} \mathbf{x}_r(0) + \int_0^t e^{s(\mathbf{W}^* - \mathbf{I})} \sin(\omega(t-s)) \mathbf{m}_c \, ds \\ &= e^{-t} e^{t\mathbf{W}^*} \mathbf{x}_r(0) + \int_0^t e^{-s} \sin(\omega(t-s)) e^{s\mathbf{W}^*} \mathbf{m}_c \, ds. \end{aligned} \quad (34)$$

Here, $\mathbf{W}^* = \alpha(\mathbf{v}\mathbf{u}^\top - \mathbf{u}\mathbf{v}^\top)$ is of rank-2 anti-symmetric transform, so considering a flow defined by $e^{t\mathbf{W}^*} \mathbf{x}_0$ with non-trivial $\mathbf{x}_0 \in S = \text{Span}\{\mathbf{u}, \mathbf{v}\}$ is purely rotational on S for $\mathbf{x}_0 \in S$. More specifically,

$$e^{t\mathbf{W}^*} \mathbf{x}_0 = \cos \lambda^* t \mathbf{x}_0 + \sin \lambda^* t \mathbf{x}_{0\wedge}, \quad \text{where } \mathbf{x}_0, \mathbf{x}_{0\wedge} \in S \quad (35)$$

with such $\mathbf{x}_{0\wedge} \perp \mathbf{x}_0$ satisfying $\|\mathbf{x}_{0\wedge}\| = \|\mathbf{x}_0\|$, and λ^* being the magnitude of only imaginary eigenvalue(which is in pair) of \mathbf{W}^* . Now decomposing \mathbf{m}_c into $\mathbf{m}_c = \overline{\mathbf{m}}_c + \tilde{\mathbf{m}}_c$ where $\overline{\mathbf{m}}_c = \text{Proj}_S \mathbf{m}_c$ and $\tilde{\mathbf{m}}_c = \mathbf{m}_c - \overline{\mathbf{m}}_c$ (thus $\|\tilde{\mathbf{m}}_c\| = \text{Dist}(\mathbf{m}_c, S)$, and $\tilde{\mathbf{m}}_c \perp S$), then RHS of Eq. (34) is decomposed into

$$\begin{aligned} \mathbf{x}_r(t) &= e^{-t} e^{t\mathbf{W}^*} \mathbf{x}_r(0) + \int_0^t e^{-s} \sin(\omega(t-s)) \tilde{\mathbf{m}}_c \, ds \\ &\quad + \int_0^t e^{-s} (\cos(\lambda^* s) \sin(\omega(t-s)) \overline{\mathbf{m}}_c + \sin(\lambda^* s) \sin(\omega(t-s)) \overline{\mathbf{m}}_{c\wedge}) \, ds, \end{aligned} \quad (36)$$

where $\overline{\mathbf{m}}_{c\wedge}$ is decided by $\overline{\mathbf{m}}_c$ in the means of relationship between $\mathbf{x}_{0\perp}$ and \mathbf{x}_0 in Eq. (35).

Computing the asymptotic behaviour of each integral as $t \rightarrow \infty$ and using the fact that the term $e^{-t} e^{t\mathbf{W}^*} \mathbf{x}_r(0)$ decays to $\mathbf{0}$ as $t \rightarrow \infty$, then Eq. (36) turns out to be asymptotically approaching

the following periodic function

$$\mathbf{x}_r^*(t) = \frac{1}{\sqrt{\omega^2 + 1}} \sin(\omega t - \theta) \tilde{\mathbf{m}}_c + c_{3, [\lambda^*, \omega]}(t) \bar{\mathbf{m}}_c + c_{4, [\lambda^*, \omega]}(t) \bar{\mathbf{m}}_{c\wedge}, \quad (37)$$

where $\theta = \tan^{-1} \omega$, and periodic functions $c_{3, [\lambda^*, \omega]}(t)$, $c_{4, [\lambda^*, \omega]}(t)$ are from lemma B with parameters λ^* and ω .

This $\mathbf{x}_r^*(t)$ is also a solution of Eq. (32). To show this, directly substituting Eq. (37) into Eq. (32) yields

$$\begin{aligned} & \frac{\omega}{\sqrt{\omega^2 + 1}} \cos(\omega t - \theta) \tilde{\mathbf{m}}_c + \omega c_{1, [\lambda^*, \omega]}(t) \bar{\mathbf{m}}_c + \omega c_{2, [\lambda^*, \omega]}(t) \bar{\mathbf{m}}_{c\wedge} \\ &= -\frac{1}{\sqrt{\omega^2 + 1}} \sin(\omega t - \theta) \tilde{\mathbf{m}}_c - c_{3, [\lambda^*, \omega]}(t) \bar{\mathbf{m}}_c - c_{4, [\lambda^*, \omega]}(t) \bar{\mathbf{m}}_{c\wedge} \\ &+ \frac{\lambda^*}{\nu^2} (\bar{\mathbf{m}}_c \bar{\mathbf{m}}_{c\wedge}^\top - \bar{\mathbf{m}}_{c\wedge} \bar{\mathbf{m}}_c^\top) \left(\frac{1}{\sqrt{\omega^2 + 1}} \sin(\omega t + \theta) \tilde{\mathbf{m}}_c + c_{3, [\lambda^*, \omega]}(t) \bar{\mathbf{m}}_c + c_{4, [\lambda^*, \omega]}(t) \bar{\mathbf{m}}_{c\wedge} \right) \\ &+ \sin \omega t \mathbf{m}_c, \end{aligned} \quad (38)$$

where each $c_{1, [\lambda^*, \omega]}(t)$, $c_{2, [\lambda^*, \omega]}(t)$ arises from the differentiation of $c_{3, [\lambda^*, \omega]}(t)$ and $c_{4, [\lambda^*, \omega]}(t)$ with respect to t as in lemma B-1. Also, we used the alternate representation of $\mathbf{W}^* \in \Lambda^2(S)$, as $\mathbf{W}^* = \alpha(\mathbf{v}\mathbf{u}^\top - \mathbf{u}\mathbf{v}^\top) = \frac{\lambda^*}{\nu^2} (\bar{\mathbf{m}}_c \bar{\mathbf{m}}_{c\wedge}^\top - \bar{\mathbf{m}}_{c\wedge} \bar{\mathbf{m}}_c^\top)$ with $\nu = \|\bar{\mathbf{m}}_c\|$. Now simplifying above equation by collecting the terms of each $\tilde{\mathbf{m}}_c$, $\bar{\mathbf{m}}_c$, and $\bar{\mathbf{m}}_{c\wedge}$, we get

$$\begin{aligned} & \left(\frac{\omega}{\sqrt{\omega^2 + 1}} \cos(\omega t - \theta) + \frac{1}{\sqrt{\omega^2 + 1}} \sin(\omega t - \theta) \right) \tilde{\mathbf{m}}_c \\ &+ (c_{1, [\lambda^*, \omega]}(t) + \omega c_{3, [\lambda^*, \omega]}(t) + \lambda^* c_{4, [\lambda^*, \omega]}(t)) \bar{\mathbf{m}}_c \\ &+ (c_{2, [\lambda^*, \omega]}(t) + \omega c_{4, [\lambda^*, \omega]}(t) - \lambda^* c_{3, [\lambda^*, \omega]}(t)) \bar{\mathbf{m}}_{c\wedge} = \sin \omega t \mathbf{m}_c. \end{aligned} \quad (39)$$

In the LHS, the coefficient of $\tilde{\mathbf{m}}_c$ is directly $\sin \omega t$, and the coefficient of $\bar{\mathbf{m}}_c$ is also equivalent to $\sin \omega t$ by lemma B-2b. On the other hand, the coefficient of $\bar{\mathbf{m}}_{c\wedge}$ is 0 by lemma B-2d. Thus the LHS is $\sin \omega t (\tilde{\mathbf{m}}_c + \bar{\mathbf{m}}_c) = \sin \omega t \mathbf{m}_c$ which is same with RHS, and this proves that the converging limit-cycle periodic motion $\mathbf{x}_r^*(t)$ of $\mathbf{x}_r(t)$ is also a solution of Eq. (32).

Now, to show statement 1, the case is that $\mathbf{m}_c \notin S_\perp$ and $\mathbf{m}_c \notin \mathcal{M}$. Then $\bar{\mathbf{m}}_c, \bar{\mathbf{m}}_{c\wedge} \neq \mathbf{0}$, and since $\bar{\mathbf{m}}_c, \bar{\mathbf{m}}_{c\wedge} \in S$, one can directly see that also $\bar{\mathbf{m}}_c, \bar{\mathbf{m}}_{c\wedge} \in \mathcal{M}$, therefore the term $c_{1, [\lambda^*, \omega]}(t) \bar{\mathbf{m}}_c + c_{2, [\lambda^*, \omega]}(t) \bar{\mathbf{m}}_{c\wedge}$ in Eq. (37) always lies in $\mathcal{M} \setminus \{\mathbf{0}\}$ because $c_{1, [\lambda^*, \omega]}(t)$ and $c_{2, [\lambda^*, \omega]}(t)$ will not vanish simultaneously for same t since $\theta_{-, [\lambda^*, \omega]} \neq \theta_{+, [\lambda^*, \omega]}$ in $c_{i, [\lambda^*, \omega]}$ by $\lambda^* > 0$. However, this means that since $\tilde{\mathbf{m}}_c \notin \mathcal{M}$, so $\mathbf{x}_r^*(t)$ belongs to $\mathcal{M} \setminus \{\mathbf{0}\}$ for only t that makes the first term of Eq. (37) to vanish, say, $t = t^\dagger$. This implies that on such time t^\dagger , we have $\mathbf{x}_r^*(t^\dagger) \in S$, and t^\dagger must satisfy $\omega t^\dagger - \theta = n\pi$, which is

$$t^\dagger = \frac{1}{\omega} \tan^{-1} \omega \mod \frac{\pi}{\omega}, \quad (40)$$

and this proves the statement 1. In contrast, if $\mathbf{m}_c \in \mathcal{M}$ whilst $\mathbf{m}_c \notin S_\perp$, then $\tilde{\mathbf{m}}_c \in \mathcal{M}$ and $\bar{\mathbf{m}}_c, \bar{\mathbf{m}}_{c\wedge} \neq \mathbf{0}$, thus resulting in $\mathbf{x}_r^*(t) \in \mathcal{M} \setminus \{\mathbf{0}\}$, $\forall t > 0$ so with $\mathbf{x}_r^*(t^\dagger) \in S$, so proving the statement 2.

On the other hand, for the case $\mathbf{m}_c \in S_\perp$ but $\mathbf{m}_c \notin \mathcal{M}$, such non-trivial \mathbf{m}_c exists when $N > n$ by the following:

Lemma C. *If $N = n$, then $S_\perp \setminus \mathcal{M} = \phi$. Otherwise, if $N > n$, then $S_\perp \setminus \mathcal{M} \neq \phi$.*

Finally, here comes the last theorem about the relationship between memory plane S and memory components \mathbf{m}_i in the main text. It proves the fact that when each memory component \mathbf{m}_i has equal lengths and mutual orthogonality, then arithmetically sampled distribution of $\{\xi_i\}_{i=1}^n$ maximizes the average storage performance of S (i.e., maximizes $\frac{1}{n} \sum_{i=1}^n \cos \theta_i$ where θ_i is the angle between each \mathbf{m}_i and S).

Theorem 3. (MAXIMUM PERFORMANCE DISTRIBUTION OF ξ_i) *Let $\{\mathbf{m}_1, \mathbf{m}_2, \dots, \mathbf{m}_n\}$ with $\mathbf{m}_i \in \mathbb{R}^N$ be the set of n -numbers of mutually orthogonal vectors (so that $N \geq n \geq 2$) having same magnitude, and $\xi_i \in \mathbb{R}$, $i = 1, \dots, n$. Define two vectors $\mathbf{u}, \mathbf{v} \in \mathbb{R}^N$ as in lemma A (i.e., $\mathbf{u} = -\Psi \sin \boldsymbol{\xi}$, $\mathbf{v} = \Psi \cos \boldsymbol{\xi}$), and let θ_i be the angle between each \mathbf{m}_i and $S \subset \mathbb{R}^N$ a 2-dimensional plane $\text{Span}\{\mathbf{u}, \mathbf{v}\}$. Then, for every possible distribution of ξ_i ,*

$$\max_{\xi_1, \dots, \xi_n} \left(\sum_{i=1}^n \cos \theta_i \right) = \sqrt{2n}, \quad (41)$$

and one possible distribution of ξ_i achieving such maximum is

$$\xi_i = \frac{i-1}{n} \pi, \quad i = 1, \dots, n, \quad (42)$$

that is, an arithmetically sequenced n -number of points in $[0, \pi]$ starting from $\xi_1 = 0$ with spacing π/n .

Proof. Suppose that $\|\mathbf{m}_i\| = l$, $\forall i$. Then, the value of $\cos \theta_i$ is equivalent to $\|\text{Proj}_S \mathbf{m}_i\|/l = \|\text{Proj}_{\text{Span}\{\mathbf{u}, \mathbf{v}\}} \mathbf{m}_i\|/l$. Now, consider a vector $\mathbf{u}_\perp \in S$ satisfying $\mathbf{u}_\perp \perp \mathbf{u}$ and $\|\mathbf{u}_\perp\| = \|\mathbf{u}\|$. Then, $\|\text{Proj}_{\text{Span}\{\mathbf{u}, \mathbf{v}\}} \mathbf{m}_i\|$ can be directly computed by only the following:

$$\|\text{Proj}_{\text{Span}\{\mathbf{u}, \mathbf{v}\}} \mathbf{m}_i\| = \sqrt{\left(\frac{\mathbf{u}_\perp^\top \mathbf{m}_i}{\|\mathbf{u}\|} \right)^2 + \left(\frac{\mathbf{u}^\top \mathbf{m}_i}{\|\mathbf{u}\|} \right)^2}. \quad (43)$$

Besides, one can see that \mathbf{u}_\perp can be explicitly represented by the terms in \mathbf{u}, \mathbf{v} as

$$\mathbf{u}_\perp = \frac{1}{\sqrt{1-\mu^2}} \left(-\mu \mathbf{u} + \frac{\eta_1}{\eta_2} \mathbf{v} \right), \quad (44)$$

where $\eta_1 = \|\mathbf{u}\|$, $\eta_2 = \|\mathbf{v}\|$, and $\mu = \mathbf{u}^\top \mathbf{v} / (\|\mathbf{u}\| \|\mathbf{v}\|)$. Therefore, substituting Eq. (44) in Eq. (43) with expressions using η_1 , η_2 and μ becomes

$$\|\text{Proj}_{\text{Span}\{\mathbf{u}, \mathbf{v}\}} \mathbf{m}_i\| = \sqrt{\frac{\left(\frac{\mathbf{u}^\top \mathbf{m}_i}{\eta_1} \right)^2 + \left(\frac{\mathbf{v}^\top \mathbf{m}_i}{\eta_2} \right)^2 - 2\mu \frac{(\mathbf{u}^\top \mathbf{m}_i)(\mathbf{v}^\top \mathbf{m}_i)}{\eta_1 \eta_2}}{1 - \mu^2}}. \quad (45)$$

Here, one can simplify expression (45) through the following: Since $\{\mathbf{m}_i\}_{i=1}^n$ is an orthogonal set, there exists an orthogonal linear transformation \mathbf{T} such that $\mathbf{T} \mathbf{m}_i = l \hat{\mathbf{e}}_i$ where $(\hat{\mathbf{e}}_i)_j = \delta_{ij}$, i.e., $\hat{\mathbf{e}}_i$ being an Euclidean canonical vector. Therefore, we can write

$$\mathbf{T} \Psi = l \mathbf{I}_{N \times n} \quad (46)$$

for some appropriately chosen \mathbf{T} where $\Psi = [\mathbf{m}_1 | \mathbf{m}_2 | \cdots | \mathbf{m}_n] \in \mathbb{R}^{N \times n}$ and $\mathbf{I}_{N \times n} \in \mathbb{R}^{N \times n}$ a matrix that only having diagonal entries with value 1. Using this fact, one can observe that $\mathbf{T}\mathbf{u} = \mathbf{T}(-\Psi \sin \xi) = -l\mathbf{I}_{N \times n} \sin \xi$, and similarly, $\mathbf{T}\mathbf{v} = \mathbf{T}(\Psi \cos \xi) = l\mathbf{I}_{N \times n} \cos \xi$, thus explicitly,

$$\begin{cases} \mathbf{T}\mathbf{u} = -l \left[\underbrace{\sin \xi_1 \quad \cdots \quad \sin \xi_n}_n \quad 0 \quad \cdots \quad 0 \right]^\top \\ \mathbf{T}\mathbf{v} = l \left[\underbrace{\cos \xi_1 \quad \cdots \quad \cos \xi_n}_n \quad 0 \quad \cdots \quad 0 \right]^\top, \end{cases} \quad (47)$$

where the zero entry part vanishes when $n = N$. Moreover, the angular preservation properties of orthogonal coordinate transform tells that

$$\text{Proj}_{\text{Span}\{\mathbf{u}, \mathbf{v}\}} \mathbf{m}_i = \text{Proj}_{\text{Span}\{\mathbf{T}\mathbf{u}, \mathbf{T}\mathbf{v}\}} (\mathbf{T}\mathbf{m}_i). \quad (48)$$

Therefore, we can suggest such change of variable with respect to transformation \mathbf{T} , i.e., $\bar{\mathbf{u}} = \mathbf{T}\mathbf{u}$, $\bar{\mathbf{v}} = \mathbf{T}\mathbf{v}$, and $\bar{\mathbf{m}}_i = \mathbf{T}\mathbf{m}_i = l\hat{\mathbf{e}}_i$ that makes Eq. (45) to be only written by the expressions in ξ_i and l , since $\bar{\mathbf{u}}$ and $\bar{\mathbf{v}}$ are only represented by ξ_i and l , from Eq. (47). After substituting above transformed expression into Eq. (45) and completing tedious simplification procedure, we finally deduce that

$$\cos \theta_i = \frac{1}{l} \|\text{Proj}_{\text{Span}\{\mathbf{u}, \mathbf{v}\}} \mathbf{m}_i\| = \frac{\sqrt{\sum_{j=1}^n \sin^2(\xi_j - \xi_i)}}{\sqrt{\sum_{\substack{j,k=1 \\ j>k}}^n \sin^2(\xi_j - \xi_k)}}, \quad (49)$$

which even having no dependence on l , the length of \mathbf{m}_i .

Now, consider the following double summation $\sum_{i,j=1}^n \sin^2(\xi_j - \xi_i)$. This is exactly sum in i performed to the square of numerator of the last term in Eq. (49). Moreover, $\sin^2(\xi_j - \xi_i) = \sin^2(\xi_i - \xi_j)$ and is zero when $j = i$, thus we read that

$$\sum_{i,j=1}^n \sin^2(\xi_j - \xi_i) = 2 \sum_{\substack{i,j=1 \\ j>i}}^n \sin^2(\xi_j - \xi_i), \quad (50)$$

which the term $\sum_{\substack{i,j=1 \\ j>i}}^n \sin^2(\xi_j - \xi_i)$ is identical the square of denominator of the last term in Eq. (49). This directly leads to the following important result:

$$\sum_{i=1}^n \cos^2 \theta_i = 2. \quad (51)$$

From this, by the corollary of Cauchy-Schwarz inequality, maximum of $\sum_{i=1}^n \cos \theta_i$ is achieved when $\cos \theta_i = \sqrt{2n}/n = \sqrt{2/n}$ for all $i = 1, \dots, n$ with value $\sqrt{2n}$, so proving Eq. (41). However, we have no idea for finding such values of ξ_i that making it happen, but we claim that such distribution of ξ_i exists, and so that the maximum of $\sum_{i=1}^n \cos \theta_i$ is achieved by choosing $\{\xi_i\}_{i=1}^n$ as in (42).

For showing this, suppose each ξ_i is chosen as (42), and first check $\bar{\mathbf{u}} \perp \bar{\mathbf{v}}$. Observe that when n is even,

$$\begin{aligned}
\bar{\mathbf{u}}^\top \bar{\mathbf{v}} &= (\mathbf{T}\mathbf{u})^\top \mathbf{T}\mathbf{v} = - \sum_{i=1}^n \sin \xi_i \cos \xi_i \\
&= - \sin \xi_1 \cos \xi_1 - \sum_{i=2}^n \sin \xi_i \cos \xi_i \\
&= 0 - \sum_{i=2}^{n/2} (\sin \xi_i \cos \xi_i + \sin \xi_{n-i+2} \cos \xi_{n-i+2}) + \sin \xi_{n/2+1} \cos \xi_{n/2+1} \\
&= - \sum_{i=2}^{n/2} (\sin \xi_i \cos \xi_i + \sin(\pi - \xi_i) \cos(\pi - \xi_i)) + \sin \frac{\pi}{2} \cos \frac{\pi}{2} \\
&= 0,
\end{aligned} \tag{52}$$

and similarly when n is odd,

$$\begin{aligned}
\bar{\mathbf{u}}^\top \bar{\mathbf{v}} &= (\mathbf{T}\mathbf{u})^\top \mathbf{T}\mathbf{v} = - \sum_{i=1}^n \sin \xi_i \cos \xi_i \\
&= - \sin \xi_1 \cos \xi_1 - \sum_{i=2}^{(n+1)/2} (\sin \xi_i \cos \xi_i + \sin \xi_{n-i+2} \cos \xi_{n-i+2}) \\
&= 0 - \sum_{i=2}^{(n+1)/2} (\sin \xi_i \cos \xi_i + \sin(\pi - \xi_i) \cos(\pi - \xi_i)) \\
&= 0.
\end{aligned} \tag{53}$$

Therefore, $\bar{\mathbf{u}} \perp \bar{\mathbf{v}}$, and the value of $\|\text{Proj}_S \mathbf{m}_i\|$ is simply $\sqrt{\left(\frac{\bar{\mathbf{u}}^\top (\mathbf{T}\mathbf{m}_i)}{\|\bar{\mathbf{u}}\|}\right)^2 + \left(\frac{\bar{\mathbf{v}}^\top (\mathbf{T}\mathbf{m}_i)}{\|\bar{\mathbf{v}}\|}\right)^2} = \sqrt{\left(\frac{\bar{\mathbf{u}}^\top (l\hat{\mathbf{e}}_i)}{\|\bar{\mathbf{u}}\|}\right)^2 + \left(\frac{\bar{\mathbf{v}}^\top (l\hat{\mathbf{e}}_i)}{\|\bar{\mathbf{v}}\|}\right)^2}$, which immediately leads to

$$\cos \theta_i = \frac{1}{l} \|\text{Proj}_S \mathbf{m}_i\| = \sqrt{\frac{\sin^2 \xi_i}{\sum_{j=1}^n \sin^2 \xi_j} + \frac{\cos^2 \xi_i}{\sum_{j=1}^n \cos^2 \xi_j}}, \quad i = 1, \dots, n. \tag{54}$$

Here, one can even show that

$$\sum_{j=1}^n \sin^2 \xi_j = \sum_{j=1}^n \cos^2 \xi_j = \frac{n}{2} \tag{55}$$

by observing the following: From Riemann integral,

$$\Delta \sum_{j=1}^n \sin^2 \xi_j \approx \int_0^\pi \sin^2 \theta \, d\theta = \frac{\pi}{2}, \quad \Delta \sum_{j=1}^n \cos^2 \xi_j \approx \int_0^\pi \cos^2 \theta \, d\theta = \frac{\pi}{2} \tag{56}$$

as $n \rightarrow \infty$ where Δ is the interval between each sampling points ξ_j , i.e., $\frac{\pi}{n}$. However, by the symmetry of functions $\cos^2 \theta$ and $\sin^2 \theta$ on interval $[0, \pi]$ and the evenly sequenced property of ξ_j , one can luckily confirm that the approximation (56) is actually an equality for all n . Thus we

finally have

$$\begin{aligned} \sum_{j=1}^n \sin^2 \xi_j &= \sum_{j=1}^n \cos^2 \xi_j = \frac{\pi}{2\Delta} \\ &= \frac{\pi}{2 \cdot \frac{\pi}{n}}, \end{aligned} \quad (57)$$

which yields Eq. (55). Therefore, we can now write Eq. (54) simply as

$$\cos \theta_i = \sqrt{\frac{2(\sin^2 \xi_i + \cos^2 \xi_i)}{n}} = \sqrt{\frac{2}{n}}, \quad i = 1, \dots, n. \quad (58)$$

This indicates that $\cos \theta_i$ is constant throughout every $i = 1, \dots, n$ with value $\sqrt{\frac{2}{n}}$, and so is $|\theta_i| = \cos^{-1} \left(\sqrt{\frac{2}{n}} \right)$. Thus above choice of $\{\xi_i\}_{i=1}^n$ achieves $\max_{\xi_1, \dots, \xi_n} \left(\sum_{i=1}^n \cos \theta_i \right) = \sqrt{2n}$. \square

Below table shows the value of $\frac{1}{n} \sum_{i=1}^n \cos \theta_i = \sqrt{\frac{2}{n}}$ for ξ_i chosen as (42) for some $n \geq 2$.

$n (\geq 2)$	2	3	4	5	6	7	8	9	10
$\max_{\xi_i} \left(\frac{1}{n} \sum_{i=1}^n \cos \theta_i \right)$	1.0000	0.8165	0.7071	0.6325	0.5774	0.5345	0.5000	0.4714	0.4472

Table 1: The value of maximum $\frac{1}{n} \sum_{i=1}^n \cos \theta_i$ for some $n (\geq 2)$. The higher the value, the better the expected performance in memory retrieval of the memory plane S , respect to each original memory components \mathbf{m}_i .

As a remark, for above such maximum performance distribution (42) of ξ_i , one can analogously deduce that for general choice of set $\{\mathbf{m}_i\}_{i=1}^n$ (i.e., \mathbf{m}_i 's are not necessarily mutually orthogonal), each θ_i between resulting S and respective \mathbf{m}_i should satisfy

$$|\theta_i| \leq \cos^{-1} \left(\sqrt{\frac{2}{n}} \right), \quad i = 1, \dots, n \quad (59)$$

as in the Eq. (8) of the main text.

S3 Stability Analysis of Steady Synaptic Solution via Computation of Maximal Lyapunov Exponents

This section contains materials for the stability analysis of the steady synaptic solution Eq. (18) of Eq. (16). Method of analysis is performed with the estimation of Lyapunov exponents (LE). Lyapunov exponent(LE) is a quantity that characterizes the rate of separation of infinitesimally close trajectories of a dynamical system [1, 2].

Conventional stability analysis starts with considering a deviation $\delta\mathbf{x}$ and $\delta\mathbf{W}$ from our target reference trajectory Eq. (18), i.e., $\mathbf{x}^*(t)$ and \mathbf{W}^* , and the main strategy is to track the tendency of exponential growth or death of each deviation. We can write such deviated trajectory as $\mathbf{x}(t) = \mathbf{x}^*(t) + \delta\mathbf{x}(t)$ and $\mathbf{W}(t) = \mathbf{W}^* + \delta\mathbf{W}(t)$. By using original equation (16), we acquire the evolution rule of each deviation by such following differential equation (which is called a variational equation);

$$\begin{cases} \dot{\delta\mathbf{x}} = (-\mathbf{I} + \mathbf{W}^*) \delta\mathbf{x} + \delta\mathbf{W}\mathbf{x}^* \\ \dot{\delta\mathbf{W}} = -\gamma \delta\mathbf{W} + \rho (\delta\mathbf{x} \mathbf{x}_\tau^{*\top} - \mathbf{x}_\tau^* \delta\mathbf{x}^\top + \mathbf{x}^* \delta\mathbf{x}_\tau^\top - \delta\mathbf{x}_\tau \mathbf{x}^{*\top}). \end{cases} \quad (60)$$

Derivation of above equation are shown at the end of this section.

Unfortunately, it is also a delay differential equation (DDE) [3] that still contains a delayed term $\delta\mathbf{x}_\tau$ of $\delta\mathbf{x}$ as the original system. Furthermore, periodic coefficients $\mathbf{x}^*(t)$ and $\mathbf{x}^*(t - \tau)$ also makes detailed analysis for measuring the growth of the deviations $(\delta\mathbf{x}(t), \delta\mathbf{W}(t))$ to be extremely difficult. In this reason, we instead tried a numerical estimation method of maximal Lyapunov exponent (MLE) using variational equation (60) while following the target reference trajectory $\mathbf{x}^*(t)$ and \mathbf{W}^* of Eq. (18).

Since (60) is a DDE, conventional computation of Lyapunov exponents for a finite-dimensional ODE [2] must be modified in order to compensate the infinite-dimensionality of DDE. One possible solution is to approximate such DDE, say, $\dot{\mathbf{x}} = f(\mathbf{x}, \mathbf{x}_\tau)$, $\mathbf{x} \in \mathbb{R}^M$ with finite dimensional discrete map $\bar{f} : \underbrace{\mathbb{R}^M \times \dots \times \mathbb{R}^M}_d \rightarrow \underbrace{\mathbb{R}^M \times \dots \times \mathbb{R}^M}_d$, with variables

$$(\bar{\mathbf{x}}^1, \dots, \bar{\mathbf{x}}^{d-1}, \bar{\mathbf{x}}^d) = (\mathbf{x}(t - (d-1)\Delta t), \dots, \mathbf{x}(t - \Delta t), \mathbf{x}(t)), \quad \left(\Delta t = \frac{\tau}{d-1} \right), \quad (61)$$

where each iteration $\bar{\mathbf{x}}^n(k+1) = \bar{f}(\bar{\mathbf{x}}^n(k))$ for $\bar{\mathbf{x}}^n$ represents the $\mathbb{R}^M \rightarrow \mathbb{R}^M$ mapping of \mathbf{x} on time t to $t + \tau + \Delta t$ [4]. For example, if ϕ_i is an initial function of Eq. (60) for \mathbf{x}_i on interval $[-\tau, 0]$, then

$$\begin{aligned} \bar{\mathbf{x}}_i(0) &= [\bar{x}_i^1(0) \quad \bar{x}_i^2(0) \quad \dots \quad \bar{x}_i^{d-1}(0) \quad \bar{x}_i^d(0)] \\ &= [\phi_i(-\tau) \quad \phi_i(-\frac{d-2}{d-1}\tau) \quad \dots \quad \phi_i(-\frac{1}{d-1}\tau) \quad \phi_i(0)]. \end{aligned} \quad (62)$$

The map starts to generate the approximated solution on interval $[\Delta t, \tau + \Delta t]$, $[\tau + 2\Delta t, 2\tau + 2\Delta t]$ and so on, from this initial value. In this manner, we are able to construct a numerically approximative discrete map \bar{f} conjugate to f (any convenient integration technique can be used). Simply for example, Euler-method integration takes

$$\begin{aligned} \bar{\mathbf{x}}^1(k+1) &= \bar{\mathbf{x}}^d(k) + f(\bar{\mathbf{x}}^d(k), \bar{\mathbf{x}}^1(k))\Delta t, \\ \text{and } 1 < i \leq d; \quad \bar{\mathbf{x}}^i(k+1) &= \bar{\mathbf{x}}^{i-1}(k+1) + f(\bar{\mathbf{x}}^{i-1}(k+1), \bar{\mathbf{x}}^i(k))\Delta t. \end{aligned} \quad (63)$$

Now, exactly same works can be done for Eq. (60). Note that it is also a DDE, the initial condition representing deviation for each component of \mathbf{x} and \mathbf{W} must be a function on interval $[-\tau, 0]$.

Let $\delta\bar{\mathbf{x}}_i(0)$ and $\delta\bar{\mathbf{W}}_{ij}(0)$ as the initial vectors for each components of the conjugate discrete map \bar{f} . Then for each iteration using integration methods like (63), we can obtain the evolution $\delta\bar{\mathbf{x}}(k)$ and $\delta\bar{\mathbf{W}}(k)$, $k \geq 1$ for each step. Then the rate of exponential growth of universal deviation (the collection of every deviations)

$$\delta[\bar{\mathbf{x}}, \bar{\mathbf{W}}](k) = [\delta\bar{\mathbf{x}}_1(k) \cdots \delta\bar{\mathbf{x}}_N(k) \delta\bar{\mathbf{W}}_{11}(k) \cdots \delta\bar{\mathbf{W}}_{NN}(k)] \in \mathbb{R}^{d(N+N^2)} \quad (64)$$

is estimated by directly computing the value

$$\lambda_{\max} = \lim_{K \rightarrow \infty} \frac{1}{K(\tau + \Delta t)} \sum_{k=1}^K \ln \left(\frac{\|\delta[\bar{\mathbf{x}}, \bar{\mathbf{W}}](k)\|}{\|\delta[\bar{\mathbf{x}}, \bar{\mathbf{W}}](k-1)\|} \right). \quad (65)$$

This value turns out to be the maximal rate of exponential evolution of the universal deviation, and is called a maximal Lyapunov exponent which convergence as $K \rightarrow \infty$ is well known [5]. Negative λ_{\max} will indicate the convergence, which indicates the local stability of $(\mathbf{x}^*, \mathbf{W}^*)$, and vice versa, positive λ_{\max} will mean instability.

Fig. 2 in page 18 shows the color plot of numerically estimated λ_{\max} under certain distribution of parameters.

Derivation of the Variational Equation

First, rewrite the original system (16) into a general form as

$$\begin{cases} \dot{\mathbf{x}} = \mathbf{f}(\mathbf{x}, \mathbf{W}) \\ \dot{\mathbf{W}} = \mathbf{g}(\mathbf{x}, \mathbf{x}_\tau, \mathbf{W}) \end{cases} \quad \text{where} \quad \begin{cases} \mathbf{f}(\mathbf{x}, \mathbf{W}) = -\mathbf{x} + \mathbf{W}\mathbf{x} + \mathbf{b}(t), \\ \mathbf{g}(\mathbf{x}, \mathbf{x}_\tau, \mathbf{W}) = -\gamma\mathbf{W} + \rho(\mathbf{x}\mathbf{x}_\tau^\top - \mathbf{x}_\tau\mathbf{x}^\top). \end{cases} \quad (66)$$

Considering deviation $\mathbf{x}(t) = \mathbf{x}^*(t) + \delta\mathbf{x}(t)$ and $\mathbf{W}(t) = \mathbf{W}^* + \delta\mathbf{W}(t)$ from reference trajectory $(\mathbf{x}^*, \mathbf{W}^*)$, we have

$$\begin{cases} \dot{\mathbf{x}}^* + \delta\dot{\mathbf{x}} = \mathbf{f}(\mathbf{x}^* + \delta\mathbf{x}, \mathbf{W}^* + \delta\mathbf{W}) \\ \dot{\mathbf{W}}^* + \delta\dot{\mathbf{W}} = \mathbf{g}(\mathbf{x}^* + \delta\mathbf{x}, \mathbf{x}_\tau^* + \delta\mathbf{x}_\tau, \mathbf{W}^* + \delta\mathbf{W}). \end{cases} \quad (67)$$

Now, applying first-ordered Taylor expansion on $(\mathbf{x}^*, \mathbf{W}^*)$ to each RHS and using $\dot{\mathbf{x}}^* = \mathbf{f}(\mathbf{x}^*, \mathbf{W}^*)$ and $\dot{\mathbf{W}}^* = \mathbf{g}(\mathbf{x}^*, \mathbf{x}_\tau^*, \mathbf{W}^*) = \mathbf{O}$, we get

$$\begin{cases} \delta\dot{\mathbf{x}} = \left. \frac{\partial \mathbf{f}}{\partial \mathbf{x}} \right|_{(\mathbf{x}^*, \mathbf{W}^*)} \cdot \delta\mathbf{x} + \left. \frac{\partial \mathbf{f}}{\partial \mathbf{W}} \right|_{(\mathbf{x}^*, \mathbf{W}^*)} : \delta\mathbf{W} \\ \delta\dot{\mathbf{W}} = \left. \frac{\partial \mathbf{g}}{\partial \mathbf{x}} \right|_{(\mathbf{x}^*, \mathbf{x}_\tau^*, \mathbf{W}^*)} \cdot \delta\mathbf{x} + \left. \frac{\partial \mathbf{g}}{\partial \mathbf{x}_\tau} \right|_{(\mathbf{x}^*, \mathbf{x}_\tau^*, \mathbf{W}^*)} \cdot \delta\mathbf{x}_\tau + \left. \frac{\partial \mathbf{g}}{\partial \mathbf{W}} \right|_{(\mathbf{x}^*, \mathbf{x}_\tau^*, \mathbf{W}^*)} : \delta\mathbf{W}, \end{cases} \quad (68)$$

where $:$ is used for the *double dot product* notation. Now computing each tensor-represented Jacobians, firstly we immediately see $\frac{\partial \mathbf{f}}{\partial \mathbf{x}} = -\mathbf{I} + \mathbf{W}$, therefore

$$\left. \frac{\partial \mathbf{f}}{\partial \mathbf{x}} \right|_{(\mathbf{x}^*, \mathbf{W}^*)} \cdot \delta\mathbf{x} = (-\mathbf{I} + \mathbf{W}^*)\delta\mathbf{x}. \quad (69)$$

For the remaining ones, observe that $\frac{\partial \mathbf{f}}{\partial \mathbf{W}}$ is a third-order tensor and each element can be found by

$$\begin{aligned}
\left(\frac{\partial \mathbf{f}}{\partial \mathbf{W}}\right)_{ijk} &= \frac{\partial f_i}{\partial W_{jk}} \\
&= \frac{\partial}{\partial W_{jk}} (W_{il} x_l), \\
&= \delta_{ij} \delta_{kl} x_l \\
&= \delta_{ij} x_k,
\end{aligned} \tag{70}$$

where the Einstein's convention for summation indices was used. Thus we have

$$\begin{aligned}
\left.\frac{\partial \mathbf{f}}{\partial \mathbf{W}}\right|_{(\mathbf{x}^*, \mathbf{W}^*)} : \delta \mathbf{W} &= \delta_{ij} x_k^* (\mathbf{e}_i \otimes \mathbf{e}_j \otimes \mathbf{e}_k) : \delta W_{lm} (\mathbf{e}_l \otimes \mathbf{e}_m) \\
&= \delta_{ij} x_k^* \delta_{jl} \delta_{km} \delta W_{lm} \mathbf{e}_i \\
&= \delta_{ij} x_k^* \delta W_{jk} \mathbf{e}_i \\
&= \delta W_{ik} x_k^* \mathbf{e}_i \\
&= \delta \mathbf{W} \mathbf{x}^*.
\end{aligned} \tag{71}$$

By similar computation, below table of equations show the computation of rest of each three terms including Jacobian tensor in the equation of $\delta \dot{\mathbf{W}}$.

$ \begin{aligned} \left(\frac{\partial \mathbf{g}}{\partial \mathbf{x}}\right)_{ijk} &= \frac{\partial g_{ij}}{\partial x_k} \\ &= \frac{\partial}{\partial x_k} \rho(x_i x_{j\tau} - x_{i\tau} x_j) \\ &= \rho(\delta_{ik} x_{j\tau} - \delta_{jk} x_{i\tau}), \\ \therefore \left.\frac{\partial \mathbf{g}}{\partial \mathbf{x}}\right _{(\mathbf{x}^*, \mathbf{x}_\tau^*, \mathbf{W}^*)} \cdot \delta \mathbf{x} \\ &= \rho(\delta_{ik} x_{j\tau}^* - \delta_{jk} x_{i\tau}^*) (\mathbf{e}_i \otimes \mathbf{e}_j \otimes \mathbf{e}_k) \\ &\quad \cdot \delta x_l \mathbf{e}_l \\ &= \rho(\delta_{ik} x_{j\tau}^* - \delta_{jk} x_{i\tau}^*) \delta_{kl} \delta x_l (\mathbf{e}_i \otimes \mathbf{e}_j) \\ &= \rho(\delta_{ik} \delta x_k x_{j\tau}^* - \delta_{ik} \delta x_k x_{i\tau}^*) (\mathbf{e}_i \otimes \mathbf{e}_j) \\ &= \rho(\delta x_i x_{j\tau}^* - \delta x_j x_{i\tau}^*) (\mathbf{e}_i \otimes \mathbf{e}_j) \\ &= \rho(\delta \mathbf{x} \mathbf{x}_\tau^{*\top} - \mathbf{x}_\tau^* \delta \mathbf{x}^\top). \end{aligned} $	$ \begin{aligned} \left(\frac{\partial \mathbf{g}}{\partial \mathbf{x}_\tau}\right)_{ijk} &= \frac{\partial g_{ij}}{\partial x_{k\tau}} \\ &= \frac{\partial}{\partial x_{k\tau}} \rho(x_i x_{j\tau} - x_{i\tau} x_j) \\ &= \rho(\delta_{jk} x_i - \delta_{ik} x_j), \\ \therefore \left.\frac{\partial \mathbf{g}}{\partial \mathbf{x}_\tau}\right _{(\mathbf{x}^*, \mathbf{x}_\tau^*, \mathbf{W}^*)} \cdot \delta \mathbf{x}_\tau \\ &= \rho(\delta_{jk} x_i^* - \delta_{ik} x_j^*) (\mathbf{e}_i \otimes \mathbf{e}_j \otimes \mathbf{e}_k) \\ &\quad \cdot \delta x_{l\tau} \mathbf{e}_l \\ &= \rho(\delta_{jk} x_i^* - \delta_{ik} x_j^*) \delta_{kl} \delta x_{l\tau} (\mathbf{e}_i \otimes \mathbf{e}_j) \\ &= \rho(\delta_{jk} \delta x_{k\tau} x_i^* - \delta_{ik} \delta x_{k\tau} x_j^*) (\mathbf{e}_i \otimes \mathbf{e}_j) \\ &= \rho(\delta x_{j\tau} x_i^* - \delta x_{i\tau} x_j^*) (\mathbf{e}_i \otimes \mathbf{e}_j) \\ &= \rho(\mathbf{x}^* \delta \mathbf{x}_\tau^\top - \delta \mathbf{x}_\tau \mathbf{x}^{*\top}). \end{aligned} $	$ \begin{aligned} \left(\frac{\partial \mathbf{g}}{\partial \mathbf{W}}\right)_{ijkl} &= \frac{\partial g_{ij}}{\partial W_{kl}} \\ &= \frac{\partial}{\partial W_{kl}} (-\gamma W_{ij}) \\ &= -\gamma \delta_{ik} \delta_{jl}, \\ \therefore \left.\frac{\partial \mathbf{g}}{\partial \mathbf{W}}\right _{(\mathbf{x}^*, \mathbf{x}_\tau^*, \mathbf{W}^*)} : \delta \mathbf{W} \\ &= -\gamma \delta_{ik} \delta_{jl} (\mathbf{e}_i \otimes \mathbf{e}_j \otimes \mathbf{e}_k \otimes \mathbf{e}_l) \\ &\quad : \delta W_{mn} (\mathbf{e}_m \otimes \mathbf{e}_n) \\ &= -\gamma \delta_{ik} \delta_{jl} \delta_{km} \delta_{ln} \delta W_{mn} (\mathbf{e}_i \otimes \mathbf{e}_j) \\ &= -\gamma \delta_{ik} \delta_{jl} \delta W_{kl} \\ &= -\gamma \delta W_{ij} (\mathbf{e}_i \otimes \mathbf{e}_j) \\ &= -\gamma \delta \mathbf{W}. \end{aligned} $
--	---	---

Therefore summing up the results for each terms, we finally get

$$\begin{cases} \delta \dot{\mathbf{x}} = (-\mathbf{I} + \mathbf{W}^*) \delta \mathbf{x} + \delta \mathbf{W} \mathbf{x}^* \\ \delta \dot{\mathbf{W}} = -\gamma \delta \mathbf{W} + \rho(\delta \mathbf{x} \mathbf{x}_\tau^{*\top} - \mathbf{x}_\tau^* \delta \mathbf{x}^\top + \mathbf{x}^* \delta \mathbf{x}_\tau^\top - \delta \mathbf{x}_\tau \mathbf{x}^{*\top}), \end{cases} \tag{72}$$

which is the variational equation, Eq. (60).

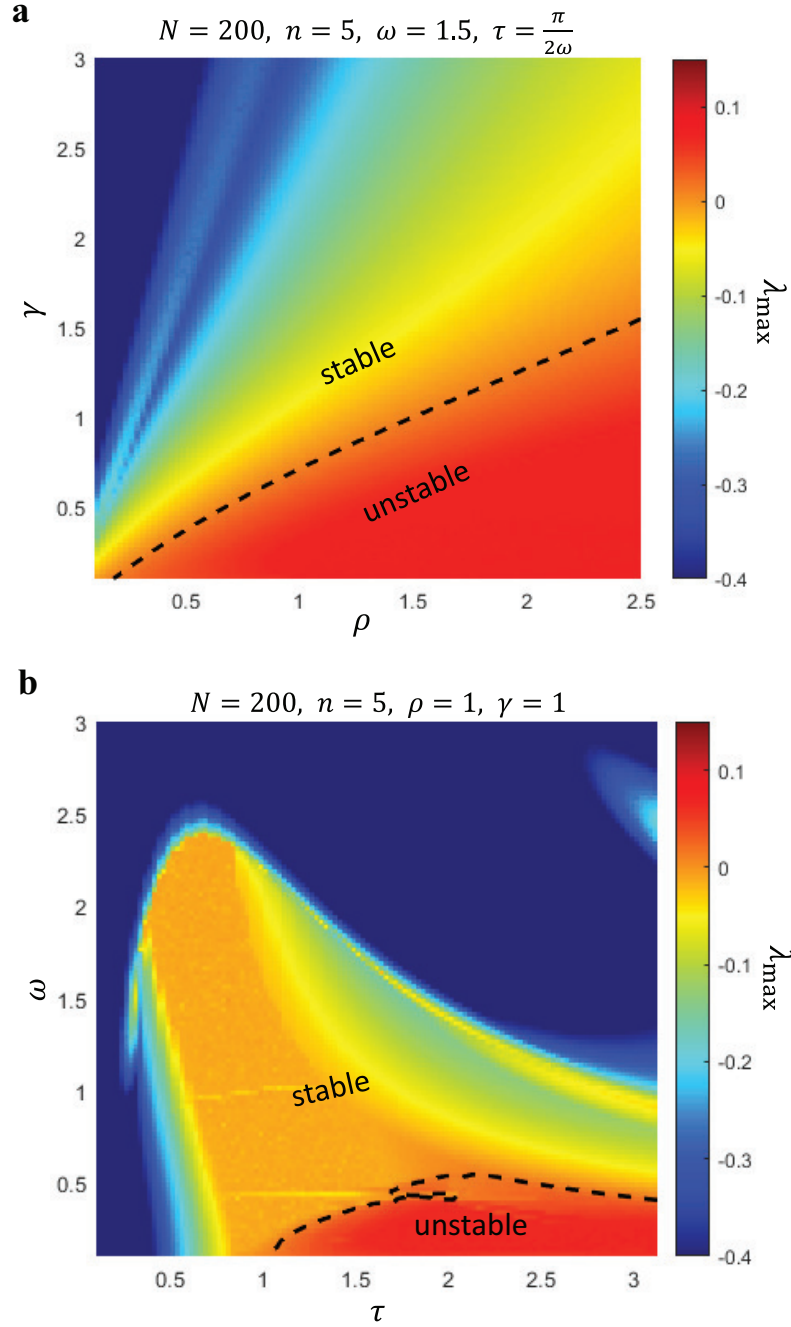


Figure 2: Plot of numerically estimated maximal Lyapunov exponent of steady state solution of \mathbf{W} in storage phase. **(a)** Color plot of λ_{\max} for parameter $(\rho, \gamma) \in [0.1, 2.5] \times [0.1, 3]$ for system with number of nodes $N = 200$ under input of 5 unit length normalized memory components and $\omega = 1.5, \tau = \frac{\pi}{2\omega}$. The unstable region tends to be confined in $\gamma \leq \alpha\rho$ for some $\alpha \approx 0.7$. **(b)** Plot of λ_{\max} for parameter $(\tau, \omega) \in [0.1, \pi] \times [0.1, 3]$ for system with number of nodes $N = 200$ under input of 5 unit length normalized memory components and $\gamma = \rho = 1$. For both plot, generally, the stable/unstable regions are hardly affected by the size of the system N . On the other hand, unstable regions tends to grow larger if the size of the input $\mathbf{b}(t)$ (or analogously, the number of memory components n) increases.

References

- [1] J. C. Sprott, *Chaos and time-series analysis*, vol. 69. Citeseer, 2003.
- [2] M. Sandri, “Numerical calculation of lyapunov exponents,” *Mathematica Journal*, vol. 6, no. 3, pp. 78–84, 1996.
- [3] J. K. Hale, S. M. V. Lunel, L. S. Verduyn, and S. M. V. Lunel, *Introduction to functional differential equations*, vol. 99. Springer Science & Business Media, 1993.
- [4] M. Lakshmanan and D. V. Senthilkumar, *Dynamics of nonlinear time-delay systems*. Springer Science & Business Media, 2011.
- [5] J. D. Farmer, “Chaotic attractors of an infinite-dimensional dynamical system,” *Physica D: Nonlinear Phenomena*, vol. 4, no. 3, pp. 366–393, 1982.